Handbook of Polymer Science and Technology

Volume 3:
APPLICATIONS AND PROCESSING OPERATIONS

edited by

Nicholas P. Cheremisinoff

MARCEL DEKKER, INC. New York and Basel

8

Applications of Continuous Mixers

Dilhan M. Kalyon
Stevens Institute of Technology
Hoboken, New Jersey

INTRODUCTION

Mixing of various ingredients is an important task in polymer processing. Mixing operations include the blending together of a number of polymeric resins, reactive processing, and the introduction of various solid and liquid additives. Some of the commonly used additives are processing aids, crosslinking, foaming and slip agents, stabilizers, antioxidants, and pigments. Various fillers and reinforcements are also incorporated into polymers to improve costs, ultimate properties, or appearance of final product.

The diverse mixing tasks encountered in polymer processing are carried out with either batch or continuous mixers. Batch mixers include paddle, double arm, planetary, intensive internal mixers, and roll mills [1, 2]. Continuous mixers include single-screw and twin-screw extruders, single-shaft kneaders, and co-rotating disk extruders. Continuous mixers have the following advantages:

1. They generally come with interchangeable parts and are thus versatile.
2. They hold only a fraction of the load of a batch mixer at any time, while producing at the same rate.
3. They facilitate better heat transfer due to their greater surface-to-volume ratio compared to batch mixers.

4. They allow for better control of product quality.
5. Uninterrupted operation is possible with continuous mixers.

In this chapter various continuous mixers and their salient features are discussed. However, first an introduction to quantitative description of the mixing quality will be made, to be followed by a review of the basic mechanisms of mixing. These concepts will be utilized in evaluation of various types of continuous mixers.

Description of Mixing Quality (Goodness of Mixing)

Quantitative means are desirable for describing the mixing quality or goodness of mixing of a given mixture. The mixture will be taken to consist of one minor and one major component, which can be solid or liquid. When more than two components are involved, analysis can be facilitated by considering the operation as concurrent mixing of each component with the rest [3]. Quantitative descriptions can be developed upon comparison of the mixture to the most complete mixing state attainable. This "complete mixing" corresponds to statistical randomness of the ultimate particles (distinct blobs of fluid, individual particulates, etc.) of the ingredients being mixed. Mixtures can thus be described by their deviation from a completely random mixture employing conventional statistical parameters, tests of confidence, and distributions.

The approach to the quantitative description of a mixture basically involves the following steps:

1. Determine whether the mixture is random.
2. If results indicate that the mixture cannot be considered as random, characterize the scale and intensity of segregation of the mixture. These parameters describe the average distance between clumps of the same component and the average deviation of the concentration from the mean concentration.

The distribution in the randomly mixed system is given by the binomial distribution, which describes the probability, P_n, of finding x particles of the minor component in each sample consisting of n particles:

$$P_n(x) = \binom{n}{x} \Phi^x (1 - \Phi)^{n-x} \tag{1}$$

where Φ is the volume fraction of the minor component in the random mixture and the binomial coefficient is given by

$$\binom{n}{x} = \frac{n!}{x!(n - x)!} \tag{2}$$

The variance, τ^2, and the coefficient of variation, β, for the binomial distribution are given by

$$\tau^2 = \frac{\Phi(1 - \Phi)}{n} \tag{3}$$

and

$$\beta = \frac{\sqrt{\tau^2}}{\Phi} = \sqrt{\frac{1 - \Phi}{n\Phi}} \tag{4}$$

To determine if a mixture is random or not, N samples of n particles each are taken from all parts of the mixture. The concentration of each sample is then determined through analytical, spectroscopic, or optical means. The mean of the samples, $\bar{c}$, and their variance, s^2, are then determined:

$$\bar{c} = \frac{1}{N} \sum_{i=1}^{N} C_i \tag{5}$$

$$s^2 = \frac{1}{N} \sum_{i=1}^{N} (C_i - \Phi)^2 \tag{6}$$

Obviously, significant deviation of $\bar{c}$ from Φ indicates a sampling error. The ratio s^2/τ^2 is computed and compared with tabulated values of χ^2/f, chi square (χ^2) over degree of freedom (f), to test the hypothesis that the system is a random mixture. If the mixture is found not to be random, two parameters, intensity and scale of segregation, are necessary to characterize the mixture.

The intensity of segregation, I, may be defined as the coefficient of variation of the concentration in the system, defined as the quotient of the limiting value of the standard deviation of the concentration of one component divided by the average concentration, Φ [3]:

$$I = \frac{\sqrt{\tau_1^2}}{\Phi} \tag{7}$$

where

$$\tau_1^2 = \lim_{N \to \infty} \frac{1}{N} \sum_{i=1}^{N} (C_i - \Phi)^2 \tag{8}$$

In practice, only a sufficient number of samples need to be collected and analyzed to bring the variance of the samples s^2 defined by Eq. 8 to the limiting value τ_1^2. Naturally, the value of I will decrease as the goodness of mixing improves. The lowest value of I corresponds to that of a random mixture given by

$$I_{\text{random}} = \beta_{\text{random}} = \sqrt{\frac{1 - \Phi}{n\Phi}} \tag{9}$$

On the other hand, the scale of segregation, which describes the average distance between clumps of the same component, can be defined as the average distance between like interfaces in the mixture. This distance is the striation thickness, r, defined as

$$r = \frac{V}{A/2} \tag{10}$$

where V is the volume and A is the interfacial area. The scale of segregation should decrease as mixing progresses, and as the interfacial area between components, A, increases. The reduction in striation thickness of a fluid system located between parallel plates and with interfaces initially oriented perpendicular to the fluid streamlines is illustrated in Figure 1. The initial striation thickness before shearing is r_i. As angle ϕ in-

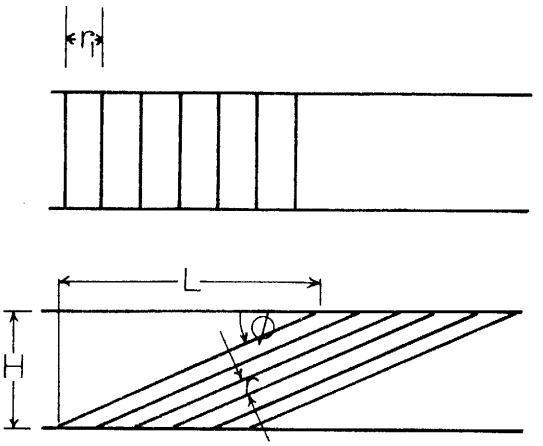

Figure 1 Reduction in striation thickness on the introduction of total strain L/H in simple shear. (From Ref. 4.)

creases, with the displacement of the top plate by a distance L to the right, the striation thickness decreases to

$$\frac{r}{r_i} = \sin \phi \tag{11}$$

Danckwerts has proposed another measure of the scale of segregation, analogous to the scale of turbulence used in fluid mechanics [5].

This measure is based on the coefficient of correlation $R(r)$, defined as

$$R(r) = \frac{1}{Ns^2} \sum_{i=1}^{N} (C'_{Ai} - \bar{C}_A)(C''_{Ai} - \bar{C}_A) \tag{12}$$

where N is the number of pairs of volume fractions (C'_{Ai}, C''_{Ai}) which are determined at a constant distance of separation r in the mixture, and $\bar{C}_A$ is the average volume fraction of component A. If $R(r)$ is determined versus the distance of separation r, a correlogram of a sample may be obtained. Typical correlograms are shown in Figure 2, for clumps of the minor component with various shapes. As mixing proceeds, the number and sizes of clumps will decrease, thus diminishing the area under the correlogram.

The analysis of a mixture for uniformity requires prior knowledge of the application of the mixture. The scale of examination or the level of scrutiny thus corresponds to the largest volume, within which a high degree of homogeneity is desired. For example in the production of multivitamin pills, the mixture of vitamins is required to be homogeneous at the scale of the volume of individual pills.

Basic Mixing Mechanisms

The mixing step may be extensive (distributive) or intensive (dispersive) in character. In extensive mixing two or more starting components are interspersed in space with one another. On the other hand, intensive (dispersive) mixing describes multitude of processes

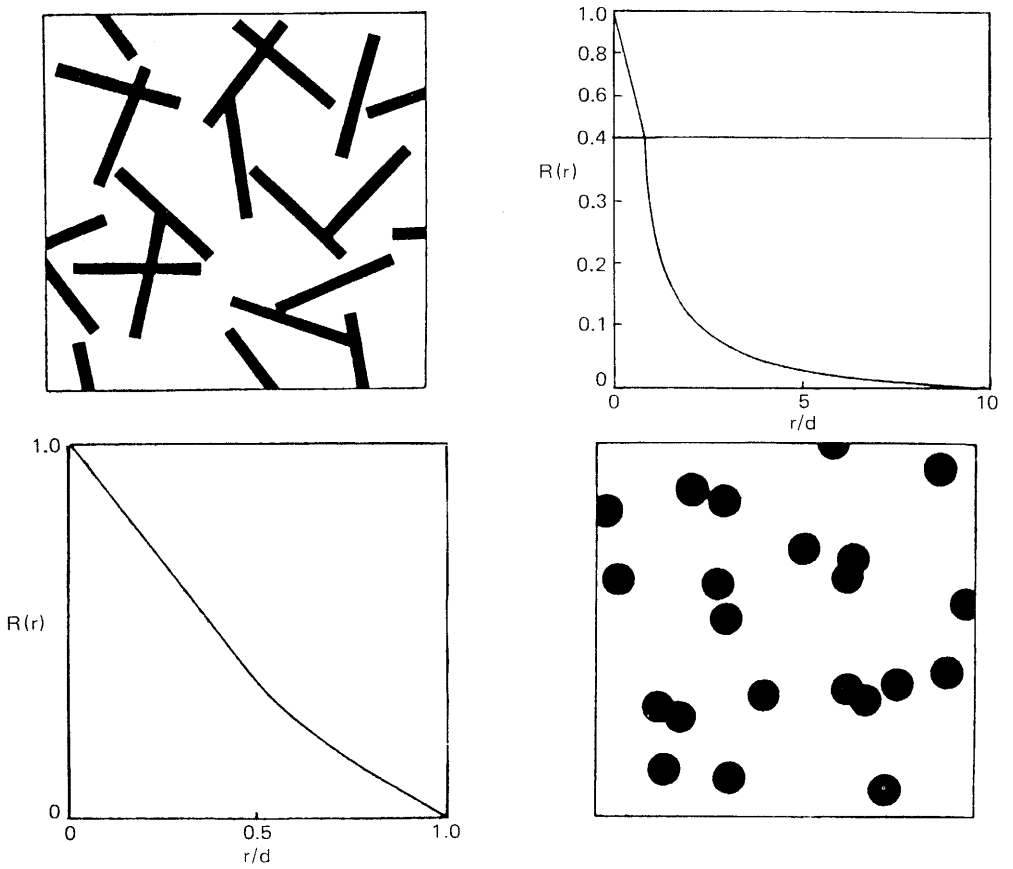

Figure 2 Correlograms for scale of segregation describing mixtures of uniform-sized spheres and strips. Diameter of spheres and width of strips is d, and length of strips is $10d$. (From Ref. 3.)

in which some intrinsic change takes place in the physical character of one or more components during processing. The extensive and intensive mixing modes are illustrated in Figures 3 and 4 with two components A and B. In Figure 3, two initially segregated liquids are shown to be mixed by distribution. Figure 4 shows schematically the process of dispersive mixing where the solid agglomerates are ruptured into their aggregates and ultimate particles. The bulk convection mixing of powder, chunks of materials, and so on, will not be considered here.

The extensive and dispersive mechanisms of mixing of polymeric viscous fluids in polymer processing differ considerably from the mixing modes available to chemical technologies for mixing of low-viscosity liquids. Diffusion and turbulence provide randomizing phenomena in the process of mixing of low-viscosity materials, which are not available to viscous liquids. On the other hand, distributive and dispersive mixing operations of viscous liquids rely on complex, continuous deformations. Thus the mechanisms of mixing of polymeric viscous liquids are inherently different in character than the mixing of inviscid fluids and necessitate special mixers.

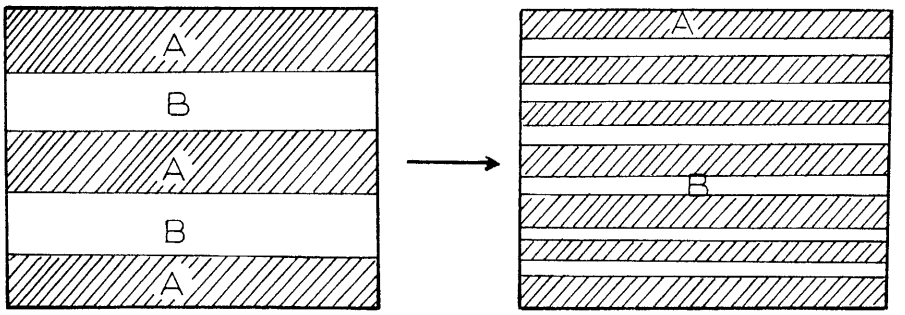

Figure 3 Extensive mixing: distribution of a minor component.

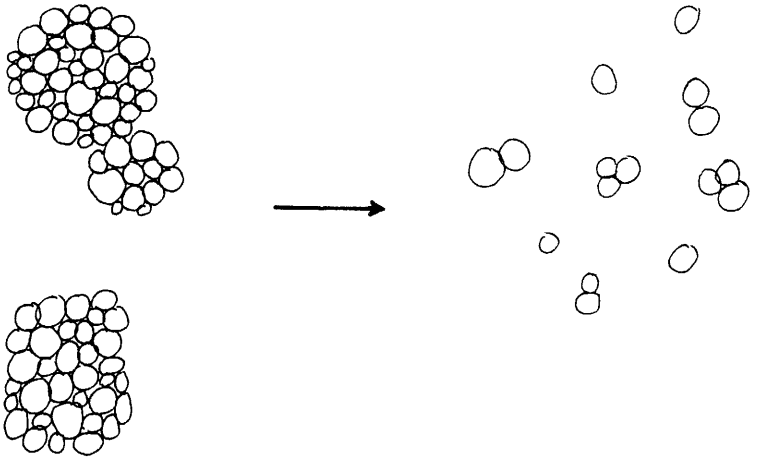

Figure 4 Intensive mixing: dispersion of solid agglomerates.

Extensive Mixing

In extensive mixing, the total strain introduced through various types of deformation (i.e., shear, squeezing, and extensional flow) induce an increase of the interfacial area between components. The interfacial area increase, in turn, reduces the striation thickness on the basis of Eq. 10.

The mechanism of extensive mixing can be understood by following a simplified analysis [3, 6]. Figure 5 shows a surface element which has been confined between two vectors $\mathbf{r}_1$ and $\mathbf{r}_2$ at time $t = 0$. The area of the surface element is given by

$$A_0 = \frac{1}{2}(C_x^2 + C_y^2 + C_z^2)^{1/2} \tag{13}$$

where C_x, C_y, C_z are the components of the vector $\mathbf{C}$, normal to the surface element (i.e., $\mathbf{C} = \mathbf{r}_1 \times \mathbf{r}_2$) and its orientation in space specified by its three directional cosines defined by

$$\cos \alpha_x = \frac{C_x}{|\mathbf{C}|} \qquad \cos \alpha_y = \frac{C_y}{|\mathbf{C}|} \qquad \cos \alpha_z = \frac{C_z}{|\mathbf{C}|} \tag{14}$$

This surface element is subjected to simple shear flow. In simple shear only one velocity component exists and this component of velocity changes in only one direction. In Figure 5, $\partial V_x/\partial y = \dot{\gamma}_{xy}$ and $V_x = \dot{\gamma}_{yx}y$.

As shown in Figure 5, after a certain elapsed time Δt, the new interfacial area is now confined between position vectors $\mathbf{r}_1'$ and $\mathbf{r}_2'$ and the ratio of the new interfacial area A to the previous area, A/A_0, becomes

$$\frac{A}{A_0} = (1 - 2 \cos \alpha_x \cos \alpha_y \gamma + \cos^2 \alpha_x \gamma^2)^{1/2} \tag{15}$$

where γ is the total strain imposed on the element during Δt, that is,

$$\gamma = \int_0^{\Delta t} \dot{\gamma}_{yx}(t')\, dt' \tag{16}$$

Equation 15 suggests that:

1. Deformed surface is proportional to the undeformed surface.
2. The total strain imposed during deformation, γ, increases the interfacial area.
3. The growth of the interfacial area depends on the orientation of the surface prior to deformation.

For large deformations where $\cos^2 \alpha_x \gamma^2 \gg 1 - 2 \cos \alpha_x \cos \alpha_y \gamma$, the interfacial area growth becomes a linear function of the total strain as

$$\frac{A}{A_0} = |\cos \alpha_x| \, \gamma \tag{17}$$

Effect of Initial Orientation on Mixing Efficiency. As suggested by Eqs. 15–17, the initial orientation of the interface between various components relative to the flow streamlines in the mixer is of paramount importance [3]. With some processing equipment, mixing efficiency can be improved drastically by proper initial placement of the compo-

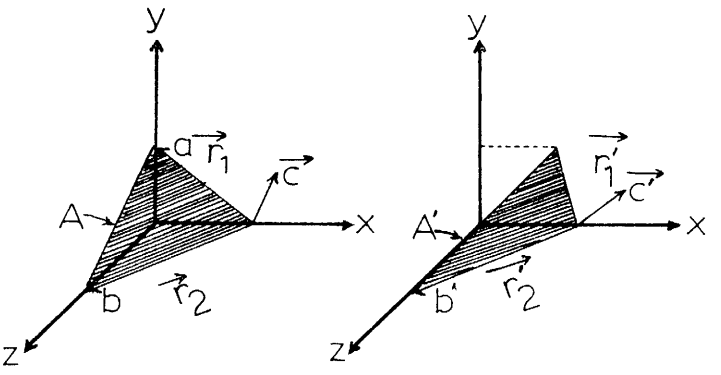

Figure 5 Change in interfacial area upon unidirectional shear strain. (From Ref. 4.)

nents. The initial placement should be such as to provide the maximum rate of increase of the interfacial surface by the flow streamlines. Thus the striation thicknesses are reduced more rapidly.

This is illustrated in Figure 6, where Couette flow is considered. In this geometry the inner shaft is rotating and the outer is cylinder stationary. Two fluids labeled A and B fill the annular gap. If the minor component, fluid A is placed as in Figure 6a, the shearing rapidly increases the interfacial area. For this initial orientation cos α_x is unity, thereby producing rapid increase in interfacial area with increasing total strain. On the other hand, Figure 6b and c show initial orientations of fluid A in which cos α_x is zero. Subsequent shearing does not produce any increase in interfacial area. Both fluids move in closed streamlines, and thus mixing relies solely on diffusion, which is a very slow process for viscous polymeric fluids.

Improvements of Interfacial Area Growth. Extensive mixing should occur more readily in shear if the simple shear flow described above is interrupted and the fluid reoriented [7]. As shown in Figure 7, where the interfacial area is determined experimentally by striation thickness measurements in a Couette geometry, the interfacial area increases with the number of times the interface is reoriented favorably for subsequent shear. The optimum reorientation of the interface is to be perpendicular to the shearing plane, as suggested by Eq. 17. For a simple shear mixer with $N - 1$ mixing sections, each of which optimizes the interfacial orientation for subsequent shear, and having N shearing sections each of equal shearing magnitude (γ/N), the growth of the interfacial area is given by [8]

$$\frac{A}{A_0} = \left(\frac{\gamma}{N}\right)^N \tag{18}$$

Upon comparison with Eq. 17, one notes that the rate of mixing with shear increases substantially by reorientations incorporated in a mixer.

So far, we have dealt with only simple shear flow. Another class of flows that one can consider is the shear free flow, for which it is possible to select for every fluid element an orthogonal set of unit vectors fixed in the element. Referred to these axes, the rate-of-strain tensor has only diagonal components [9].

$$\underline{\underline{\dot{\gamma}}} = \begin{pmatrix} \dot{\gamma}_{11} & 0 & 0 \\ 0 & \dot{\gamma}_{22} & 0 \\ 0 & 0 & \dot{\gamma}_{33} \end{pmatrix} \tag{19}$$

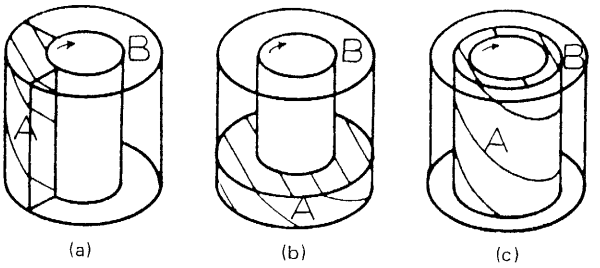

Figure 6 Effect of initial orientation on extensive mixing. (From Ref. 3.)

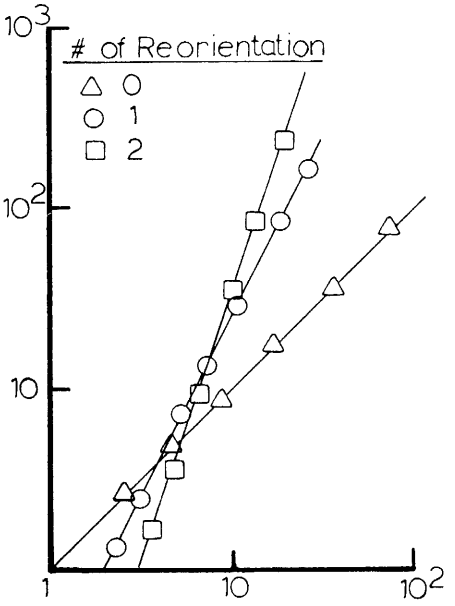

Figure 7 Effect of interface reorientation on mixing efficiency. (From Ref. 7.)

The uniaxial elongational flow is defined with

$$\dot{\gamma}_{11} = 2\dot{\epsilon} \qquad \dot{\gamma}_{22} = -\dot{\epsilon} \qquad \dot{\gamma}_{33} = -\dot{\epsilon}$$

where $\dot{\epsilon}$ is the uniaxial Hencky strain rate given by

$$\dot{\epsilon} = \frac{1}{L(t)} \frac{dL(t)}{dt} \tag{20}$$

and $L(t)$ is the change in total length of stretched sample. The total strain is given by

$$\epsilon = \ln \frac{L(t)}{L_0} = \ln \lambda_x \tag{21}$$

where λ_x is the extension ratio in the stretch direction.

The interfacial area grows with increasing extensional strain ϵ as [3, 7]

$$\frac{A}{A_0} = \left[\lambda_x + \cos^2 \alpha \left(\frac{1}{\lambda_x} - \lambda_x \right) \right]^{1/2} \tag{22}$$

If the interface is oriented with $\cos \alpha = 0$, then

$$\frac{A}{A_0} = \lambda_x^{1/2} = e^{\epsilon/2} \tag{23}$$

Thus extensional flows, which occur in mixing principally when the material is forced through contractions, give rise to improved efficiency in extensive mixing, compared to shear flows.

In summary, the goal of extensive mixing is to generate composition uniformity of the ingredients throughout the mixture. In this mode of mixing, large strains need to be imposed on the fluid. Furthermore, the interfacial elements (or the solid additives) need to be distributed throughout the system. The initial orientation of the phases and the subsequent orientation of the interface are critical for achieving efficient extensive mixing. Extensional flows improve the efficiency of extensive mixing processes.

It should be noted that so far we have employed a very simplified analysis in which viscoelasticity of phases, interfacial tension, filled liquid systems, and liquid drop/wall and drop/drop interactions are ignored. Information on these aspects may be found elsewhere [10–23].

Intensive Mixing and Dispersion

The mixing of solid additives into a polymeric matrix, that is, filled or reinforced plastics or rubbers generally involves the rupture of agglomerates of the solid particulates and the further separation of the closely packed particles after rupture [24, 25]. These operations constitute dispersive mixing operations in which some intrinsic change takes place (i.e., in shape and size of the particulates of solid phase).

It can be assumed that the agglomerates rupture when internal stresses, induced by viscous drag on the particles, exceed a certain threshold value [26]. This threshold may be considered as the cohesive force holding the agglomerate together. The simplified dynamics of dispersive mixing is illustrated next by considering two rigid beads of radii r_1 and r_2 present in a homogeneous flow field as shown in Figure 8 [4, 27–29]. For low Reynolds number flows, as typical in polymer processing, the viscous drag force being exerted on each spherical rigid particle of radius r_i by the Newtonian fluid of shear viscosity η is $6\pi\eta r_i$ according to Stokes' law. In simple shear flow of an incompressible, Newtonian fluid with shear rate $\dot{\gamma}$, the force between the particles can be shown to be [29]

$$F = \frac{6\pi\eta\dot{\gamma}X_2Y_2}{L}\frac{r_1r_2}{r_1 + r_2} \tag{24}$$

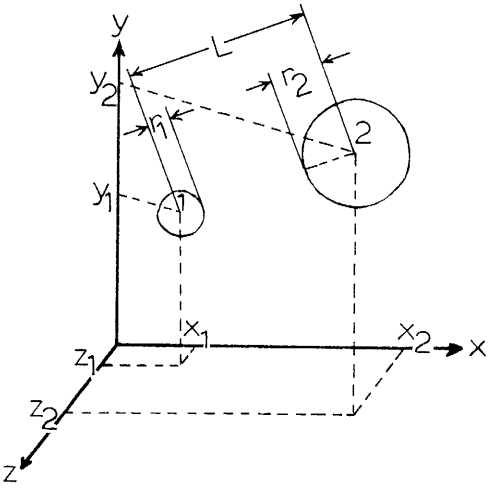

Figure 8 Two particles of radii r_1 and r_2 being separated during dispersive mixing. (From Ref. 1.)

where X_2 and Y_2 are the coordinates of the second bead with the coordinate system placed at the center of bead 1, L is the center-to-center distance between the particles, and η is the Newtonian viscosity of the fluid dragging the particles. The force between the particles vanishes when X_2 or Y_2 are zero, that is, if the line connecting the centers of the two spheres are parallel or perpendicular to the flow field [1], emphasizing as in extensive mixing the significance of the initial orientation of the agglomerate. For the case of the two rigid spheres in contact with each other, the maximum force acting to separate the spheres is

$$F_{\max} = 3\pi\eta\dot{\gamma}r_1r_2 \tag{25}$$

Equation 25 indicates that the maximum force acting to rupture an agglomerate of solid particles will be proportional to the shear stress ($\eta\dot{\gamma}$) acting on the agglomerate. Simply put, this suggests that high shear stresses promote dispersion. With a given system there is a critical value of shear stress below which no dispersion will occur. When the shear stress is above the critical value, only those which are favorably oriented with their long axis perpendicular to the streamlines will be dispersed [4]. Maximum force is also seen to increase with increasing product of radii, r_1r_2. This indicates that it is easier to break two large particles apart in comparison to one large and one small or two small particles. It should be noted, however, that this simplified analysis ignores the effects of the agglomerates on the flow kinematics and the surface chemistry and interactions between agglomerates.

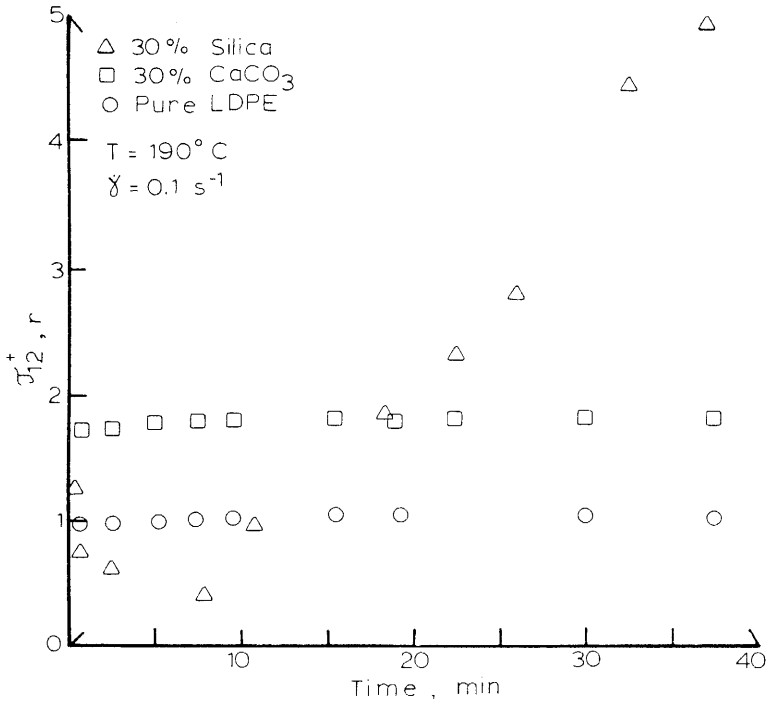

Figure 9 Shear stress growth function of a polyethylene resin filled with two different fillers.

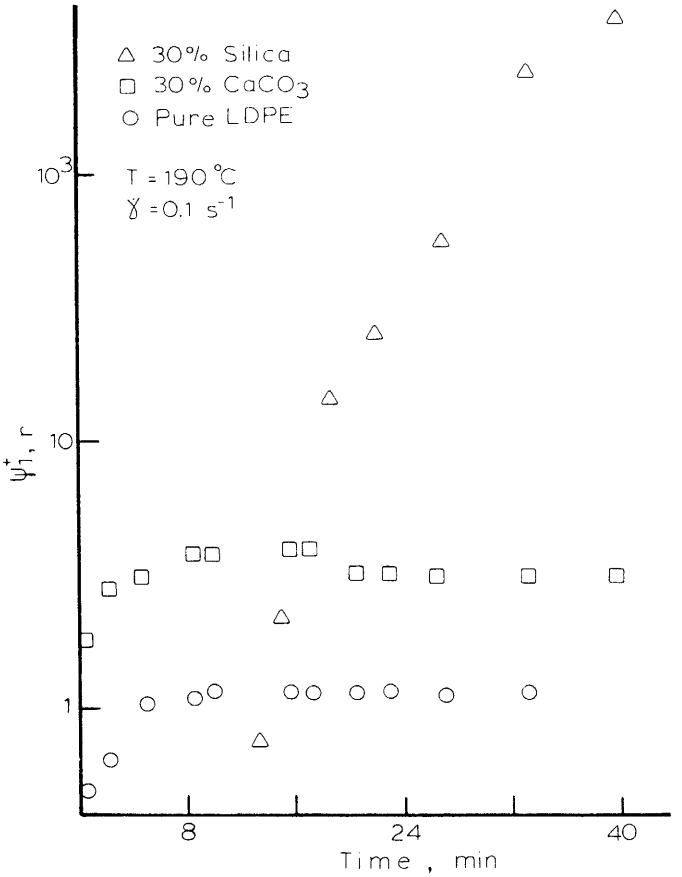

Figure 10 First normal stress difference growth function of a polyethylene resin filled with two different fillers.

Figures 9 and 10 show the comparison of the rheological behavior of a surface-treated $CaCO_3$ filler versus an untreated silica-based filler under simple shear flow in between a cone and a plate (30). Both fillers are incorporated at 30% by weight into a low-density polyethylene matrix, LDPE employing similar compounding procedures. Figure 9 shows the shear stress growth. The $\tau^{+}_{12,r}$ indicates that the shear stress values are normalized by division with the steady shear stress value exhibited by neat LDPE at 0.1 s^{-1}. On the other hand, Figure 10 drawn on a semilog graph shows the first normal stress growth material function, $\Psi^{+}_{1,r}$, normalized by division with the first normal stress coefficient of the LDPE resin at 0.1 s^{-1}. Both fillers exhibit similar particle size distribution.

The surface-treated $CaCO_3$-filled samples behave very similar to the behavior of the neat polymer, characterized by reaching of steady torque and normal force. On the other hand, steady-state shear stress and first normal stress difference values are not reached with the silica-based filler. Especially the first normal stress difference exhibits a spectacular rise with time of deformation. This suggests that agglomeration and strong inter-

action occur between agglomerates of the silica-based filler. These interactions convert the structure during simple shear into a network which approaches solidlike behavior [30], suggesting strong ramifications on the processing requirements of this filled system.

Particle attrition deserves special attention, especially in the compounding of highly filled or reinforced systems. An example to particle attrition is shown in Figure 11. Ammonium sulfate particles were compounded into a polybutadiene matrix employing a corotating twin-screw extruder. The ultimate particles of ammonium sulfate are shown to be ground up during mixing, as revealed by the scanning electron micrographs. Also, in the introduction of reinforcements, fiber attrition occurs readily and is highly undesirable, because it results in decreases in various ultimate properties.

Demixing

Demixing is an important aspect of every mixing operation. The selected geometry and flow kinematics for compounding of various ingredients may under certain situations give rise to the demixing of the ingredients. A simple example can be seen from Eq. 15, which was utilized to describe the growth of the interfacial area with increasing strain during extensive mixing. For small strains and for various initial orientations that give rise to the condition

$$2 \cos \alpha_x \cos \alpha_y \gamma > 1 + \cos^2 \alpha_x \gamma^2 \tag{26}$$

the applied strain would reduce the interfacial area contrary to our general intuitive expectations.

Demixing may occur in the blending of two incompatible liquids with differing shear viscosities, if the blend is made to undergo pressure flow. The most common situation is pressure flow through a die, where the two fluids may segregate [31–33]. This would involve the migration of the lower molecular weight and thus lower viscosity resin to the high shear rate region (i.e., toward the wall in Poiseuille flow). The higher-viscosity resin will occupy the low-shear-rate region, located at the center of the tubular die.

In mixing of suspensions, rigid particles have been observed to migrate across planes of shear in directions that depend on the rheological behavior of suspending liquid [34]. In the mixing of suspensions, incorporating a distribution of particle size of the solid phase, the smaller particles may migrate to the wall of the die, whereas the greater particles occupy the low shear rate region of the die (Segre–Silberberg effect [35–37]). Furthermore, in the mixing of highly filled suspensions, if the suspension is forced through a contraction with a steep degree of approach, the solid particulates may establish a solid bed, which effectively filters out the polymer matrix [38, 39]. Upon depletion of the polymer, the pressure builds up. This results eventually in the rupture of the solid bed with a slip at the wall. This will give rise to a product with a concentration varying as a function of time.

Components of a mixture may also demix upon the completion of the mixing and the shaping operation. Examples include the exudation of the slip additives to the surface of polymeric films, a phenomenon used to promote slip between film layers and film/metal surfaces [40, 41] and the undesired but commonly occurring exudation of the plasticizers from PVC articles with time. In general, the geometry and operating conditions should be selected to minimize the segregation of components during and after the mixing operation. Obtaining a good mixture at one point of the process is no guarantee that the state of the mixture will be conserved during the rest of the process.

(a)

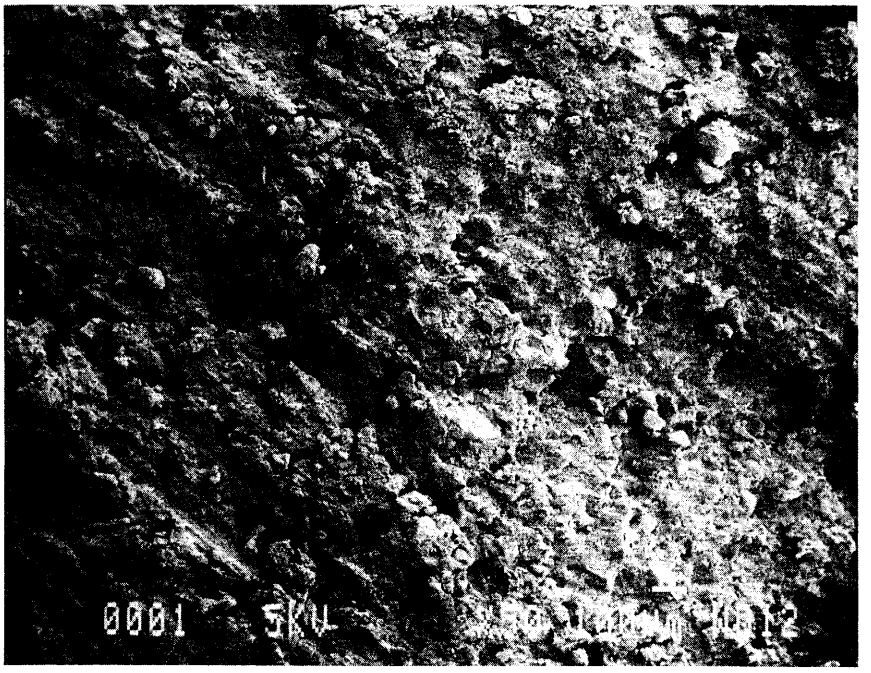

(b)

Figure 11 Scanning electron micrographs of samples filled with ammonium sulfate particles: (a) compounded properly; (b) compounded under conditions that resulted in particle attrition.

CONTINUOUS MIXERS

Basic Single-Screw Plasticating Extruder

The single-screw plasticating extruder is one of the most widely used machines in polymer processing. A plasticating extruder consists of an Archimedean screw rotating in a heated barrel, with a "head" or die attached as shown in Figure 12. Solids in the form of pellets, powder, and so on, can be fed into a plasticating extruder either through a hopper (i.e., "flood feeding") or by "starved" feeding. In flood feeding of an extruder, the feed hopper is filled with solid particles. Under the influence of gravity and the interparticle and particle/wall friction forces, the particles are fed into the extruder feed throat, where they are picked up by the rotating screw. On the other hand, solid feed can be metered into the extruder feed throat by a feeding device at controlled rates (i.e., starved feeding) [42–44].

For polymer processing operations that involve large aspect ratios and low Reynolds numbers, the system can be modeled as a stationary channel with the upper plate moving diagonally across the top at helix angle θ, as shown in Figure 13. The solids are conveyed in the down-channel direction through particle/barrel frictional drag.

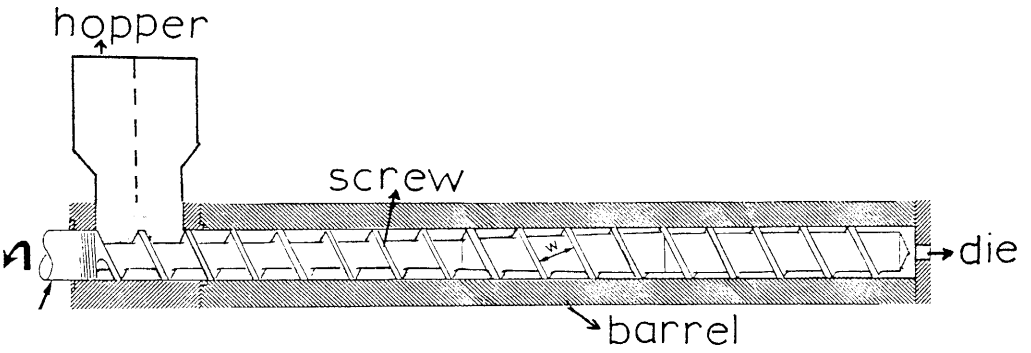

Figure 12 Plasticating single-screw extruder.

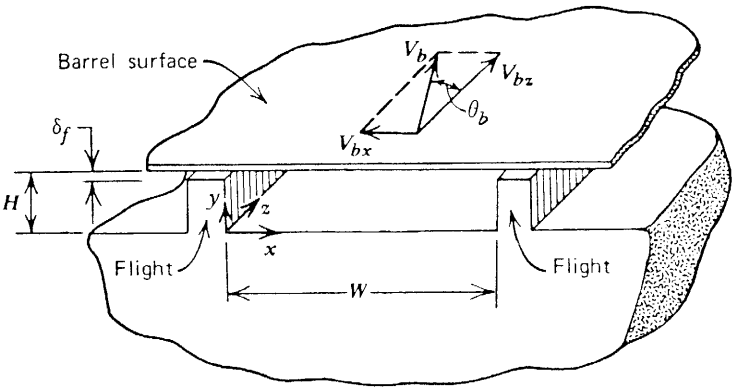

Figure 13 Schematic of unwound single-screw extruder geometry. (From Ref. 1.)

The conveying of the solids by frictional drag at the barrel is accompanied by the compaction of the deformable solid bed and increase in pressure. Friction generates heat mainly at the barrel/solid bed interface, proportional to the developed pressure and the friction coefficient of the barrel [45]. The heat generation plus the heat flux conducted through the barrel increases the temperature of the solids at the barrel/solid plug interface to above the melting temperature for semicrystalline polymers and to above the glass transition temperature for amorphous polymers.

At this location, the frictional drag mechanism is converted into a viscous drag mechanism, whereby the solid bed is conveyed further by shear stresses generated in the molten film sandwiched between the barrel and the solid plug. Examples of pressure and heat generation rate versus down-channel distance and the temperature distribution in the solid bed during solid conveying are shown in Figures 14–16, as a function of screw speed and mass flow rate related to the compounding of a thermoset powder [46].

As shown schematically in Figure 17, the pushing flight scrapes the molten layer off the barrel and the melt starts accumulating at the pushing flight. As melting proceeds, the relative width of the solid bed, X/W, gradually decreases.

Neglecting the leakage flow through the flight clearance, δ, the equation of motion for

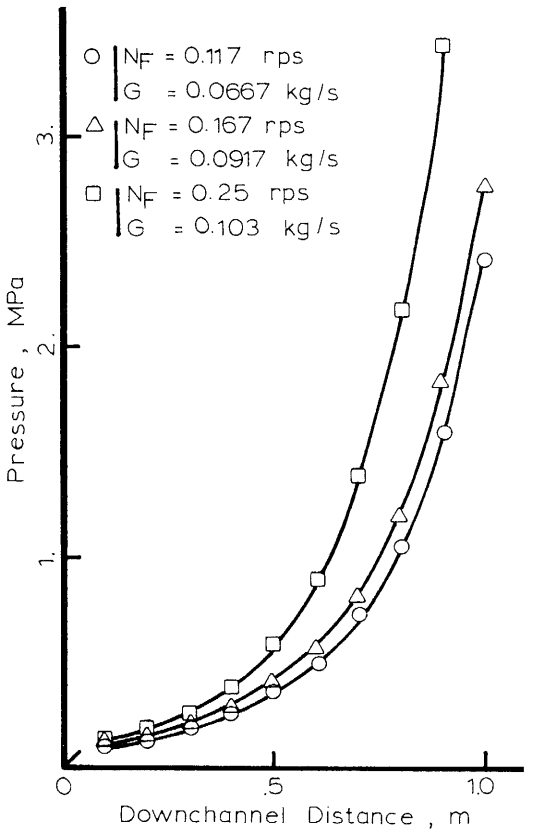

Figure 14 Pressure in the down-channel direction. (From Ref. 46.)

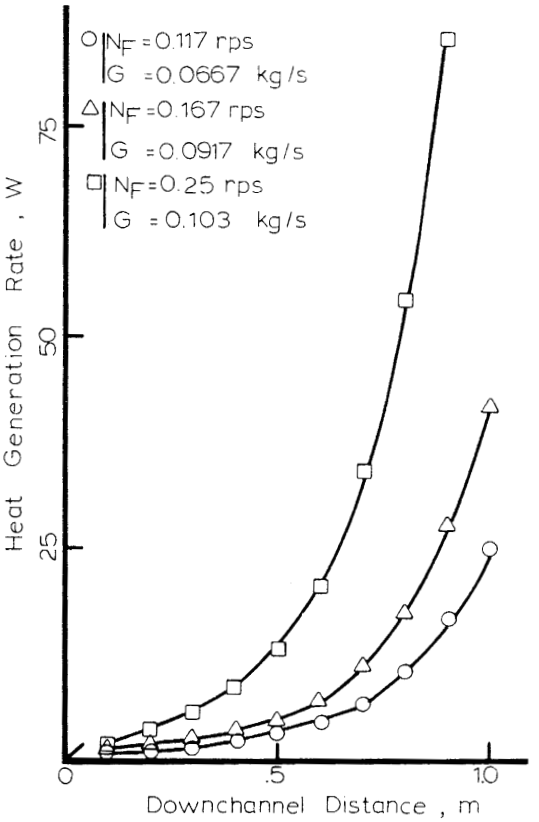

Figure 15 Heat generation rate at barrel/solid interface in down-channel direction. (From Ref. 46.)

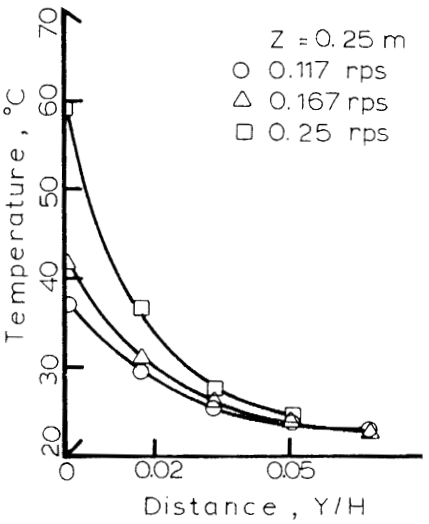

Figure 16 Temperature distributions in solid bed in down-channel direction. (From Ref. 46.)

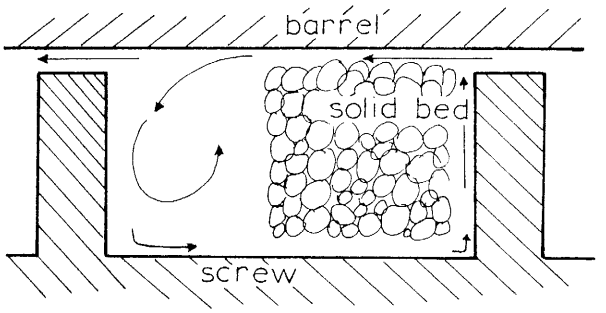

Figure 17 Schematic of melting in a single-screw extruder.

the melt pool in the cross-channel direction x for fully developed, isothermal flow of an incompressible Newtonian fluid is

$$\frac{\partial P}{\partial x} = \eta \frac{\partial^2 V_x}{\partial y^2} \tag{27}$$

which can be easily solved [4] with $V_x(0) = 0$ and $V_x(H) = -V_{bx}$ and with zero net flow rate in the x direction:

$$\int_{y=0}^{y=H} V_x \, dy = 0 \tag{28}$$

The cross-channel velocity profile becomes

$$V_x = V_{bx} \frac{y}{H}\left(2 - 3\frac{y}{H}\right) \tag{29}$$

where V_{bx} is the x component of barrel velocity, V_b, that is, $V_b \sin \theta b$, with θb the helix angle at barrel surface and H is the channel depth.

The described velocity profiles obtained with Newtonian fluids under fully developed isothermal conditions are instructional. However, for detailed calculations, one can resort to numerical techniques. The typical and realistic cross-channel velocity profile in the channel is shown in Figures 18 and 19 and describe the circulation of the melt in the melt pool while being pumped in the down-channel direction. The length of the arrow indicates the magnitude of the velocity. The curvature of the screw geometry has been taken into consideration by applying a finite-element-based numerical technique in conjunction with various types of fluids [47].

The melt pool is conveyed forward in the down-channel direction by the axial component of the drag flow induced by motion of the barrel, V_{bz}. Pressure builds up in the forward direction, due to the resistance offered by the die at the outlet of the extruder. The net volumetric flow rate in the axial direction can be given for fully developed isothermal flow of a Newtonian fluid in a constant-channel-depth H channel:

$$Q = \frac{V_{bz} WH}{z} F_d + \frac{WH^3}{12\eta}\left(\frac{-\partial P}{\partial z}\right) F_p \tag{30}$$

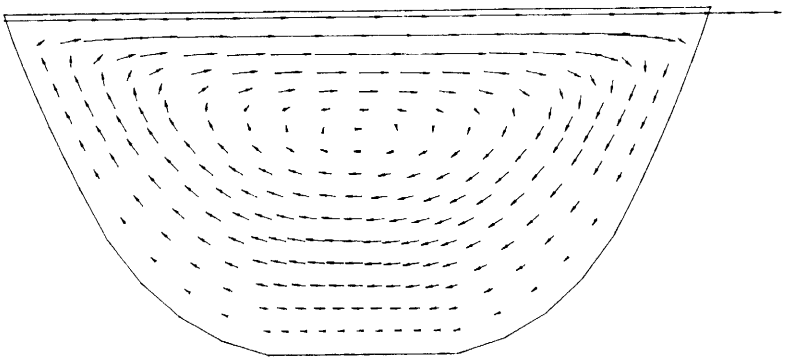

Figure 18 Cross-flow in a single-screw extruder channel with Newtonian fluids. (From Ref. 47.)

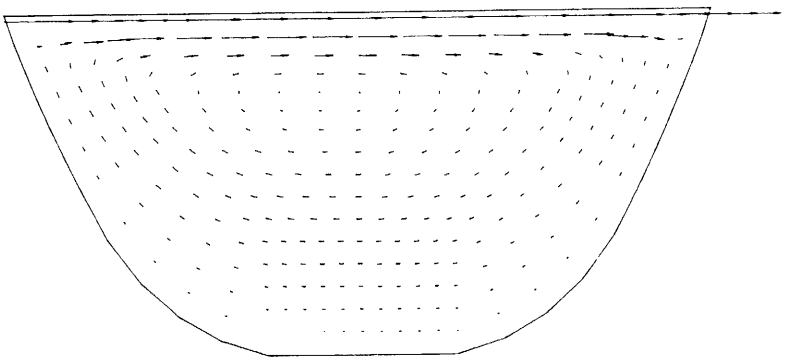

Figure 19 Crossflow in a single-screw channel with Bingham plastic. (From Ref. 47.)

where F_d and F_p are "shape factors" for the pure drag and pure pressure flows, respectively. The values of shape factors are less than 1 and depend on the aspect ratio H/W. The net flow rate in the axial direction, V_1, becomes

$$V_1 = V_x \cos\theta + V_z \sin\theta \tag{31}$$

The ratio of pressure to drag flow rates is given by

$$\frac{-Q_p}{Q_d} = \frac{H^2}{6\eta V_{bz}}\left(\frac{\partial p}{\partial z}\right)\frac{F_p}{F_d} \tag{32}$$

The net flow rate, Q, is obtained by linear superposition of drag, Q_d, and pressure, Q_p, flow rates [4], valid for isothermal, fully developed, Newtonian flow. The velocity profiles corresponding to various Q_p/Q_d values are shown in Figure 20. From these velocity profiles, one can deduce the path of fluid particles in the channel. For closed discharge, $Q_p/Q_d = -1$, the fluid advances and retreats in the x and z directions. Overall, as shown in Figure 21, the fluid particles move in a helical path through the helical channel, "helix in a helix," the helix angle at any point being determined by local velocity field.

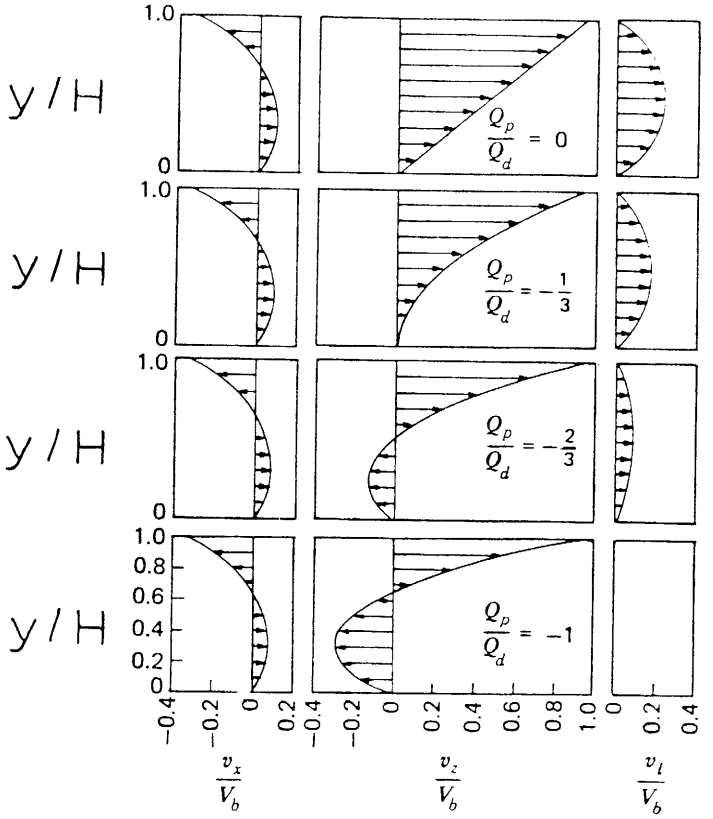

Figure 20 Cross-channel, down-channel, and axial velocity profiles for various Q_p/Q_d values in shallow, square pitched screws. (From Ref. 4.)

Obviously, fluid particles experience different strain histories according to their initial geometrical location between a screw and a barrel [1, 4, 48, 49], indicating that the extrudate leaving the extruder will not be uniformly mixed. Taking into consideration the residence-time distribution of the melt, a weighted-average strain, γ_{av}, can be defined [49] as

$$\gamma_{av} = \frac{\int_{t_0}^{t} \gamma f(t)\, dt}{\int_{t_0}^{t} f(t)\, dt} \tag{33}$$

where $f(t)\, dt$ is the fraction of the fluid, at the exit, that has spent a time between t and $t + dt$ in the extruder, t_0 is the minimum residence time pertaining to the fluid located initially at $y/H = \frac{2}{3}$. The experimental and theoretical cumulative residence-time distribution function, $F(t)$, which represents the fraction of the material that has spent the time, t, or less in the single-screw extruder, is shown in Figure 22. The mean residence time, $\bar{t}$, is given by

$$\bar{t} = \int_{t_0}^{\infty} tf(t)\, dt \tag{34}$$

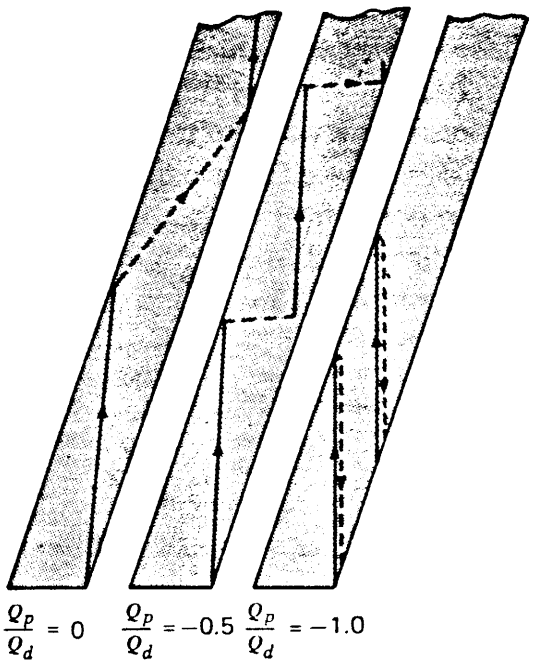

Figure 21 Path of a fluid particle in the screw channel. (From Ref. 1.)

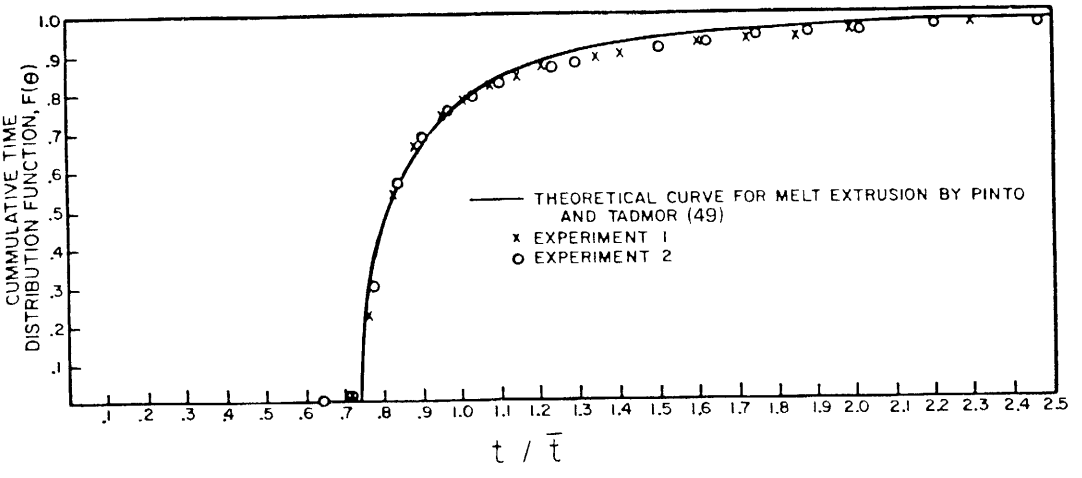

Figure 22 Experimental and theoretical cumulative residence-time distribution in a single screw. (From Ref. 50.)

The residence-time distribution in a melt extruder is quite narrow and only 5% of the flow rate stays more than twice the mean residence time in the single-screw extruder. The typical strain distribution function across the channel is shown in Figure 23 as a function of the back pressure (i.e., Q_p/Q_d ratio). The strain increases at every point as the back pressure increases [49]. The effect of helix angle on the weighted-average strain is shown in Figure 24. The average strain goes to infinity at 0° and 90° helix angles. The minimum is rather flat and covers a significant helix angle range.

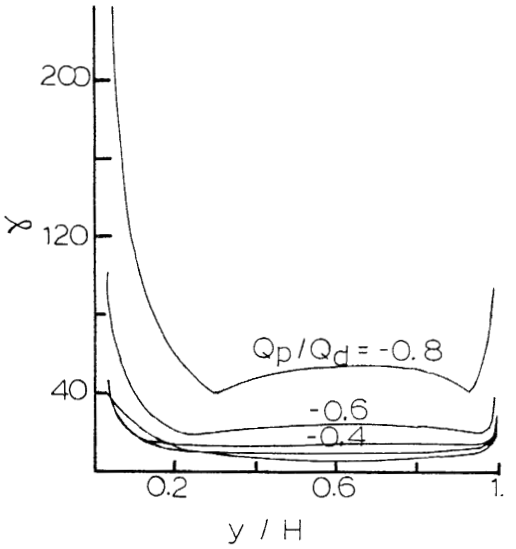

Figure 23 Strain distribution function across the channel as a function of Q_p/Q_d ratio. (From Ref. 49.)

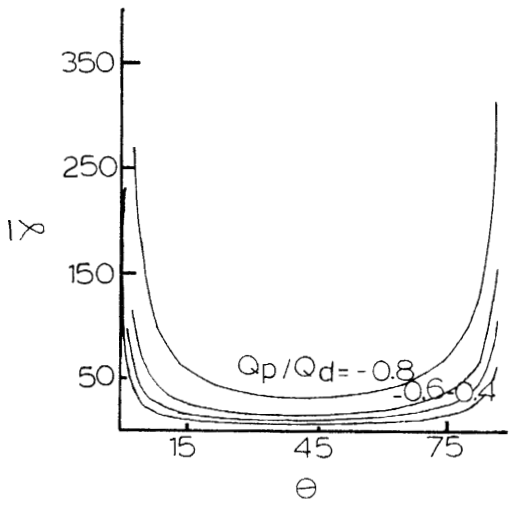

Figure 24 Weighted-average total strain, γ, as a function of helix angle at various Q_p/Q_d values. (From Ref. 49.)

It should be noted that although large strains can be imposed in single-screw extrusion through the flow kinematics described above, the lack of effective orientation of the material elements at the flights cause the bulk of the interfacial area to be oriented parallel to the channel bottom in a relatively short downstream distance, regardless of initial orientation of the components to be mixed [51]. Consequently, the extensive mixing achieved in single-screw extruders is generally poor. Furthermore, there is no dispersive mixing capability which can rupture agglomerates in a general-purpose single-screw extruder except for leakage flow over small flight clearance, δ. For better mixing either special mixing sections are incorporated into the single screw; that is, screw modifications or the design is radically altered to introduce gaps through which portions of the melt are repeatedly forced (i.e., single-shaft kneaders).

Single-Screw Extruders Modified for Better Mixing

The rapid orientation of the interfacial area parallel to the channel bottom regardless of initial orientation and the lack of effective reorientation of the interfacial area are identified as causes for the poor mixing in single-screw extruders. This has led to the design and incorporation of mixing sections. Mixing sections obstruct and disrupt the flow, thus redistributing the streamlines and reorienting the interfacial area [52–55]. Both obviously improve the extensive mixing efficiency of single-screw extruders.

The simplest mixing section that can be incorporated into plasticating extrusion is a series of mixing pins as shown in Figure 25. Each mixing pin divides the helical flow into two streams, which are again combined into one upon passing the pin. The growth of the interfacial area upon the division and combination of the flow upon passing around a mixing pin is shown in Figure 26. On the other hand, the introduction of the mixing pin introduces further velocity gradients and thus should also increase the total strain imposed on the material.

Fluted mixing sections in single-screw extruders are devices also employed to redistribute the melt, as shown in Figure 27. These barrier-type restrictions basically introduce gaps that all melt elements need to pass through [53]. The barrier may take a number of forms. A simple form is the dam or series of dams of almost the full channel height welded across the channel at selected locations. This continuous distribution of the melt, reorientation of the interface, and further shearing obviously improve the efficiency of extensive mixing in a single-screw extruder.

Potential problems with fluted mixing sections are holdup of material and dead spots [54, 55], which can be minimized by proper selection of the helix angle of this section and by tapering the inlet channel to zero depth and by reversing the depth profile in the outlet channel. There should also be considerable pressure drop as the material is forced from

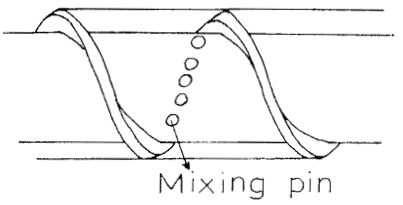

Figure 25 Mixing pins.

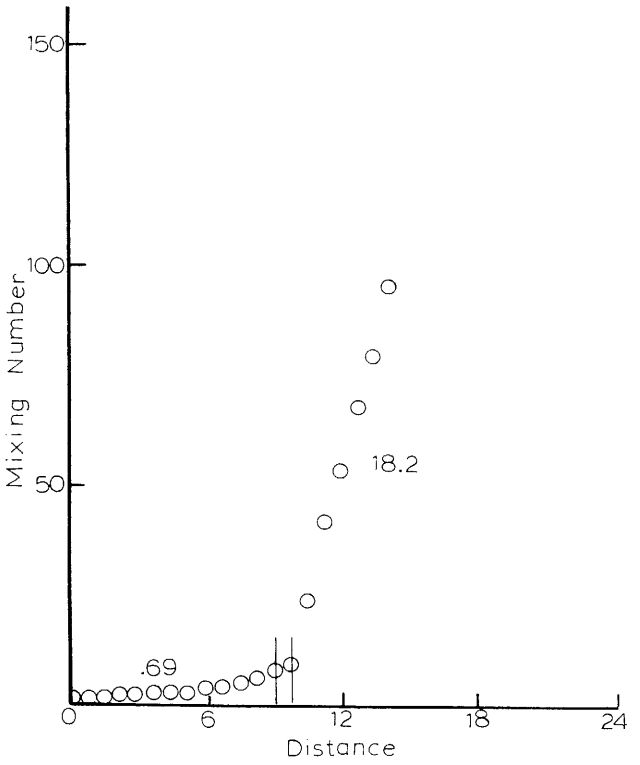

Figure 26 Growth of interfacial area upon passage around a mixing pin. (From Ref. 52.)

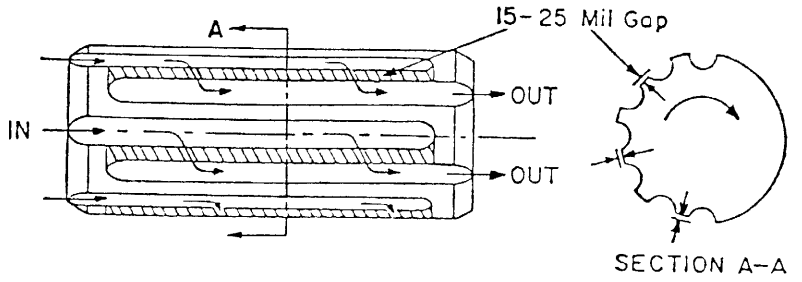

Figure 27 Fluted mixing sections.

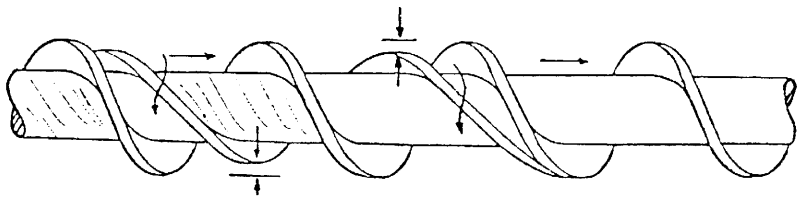

Figure 28 Maillefer transition section.

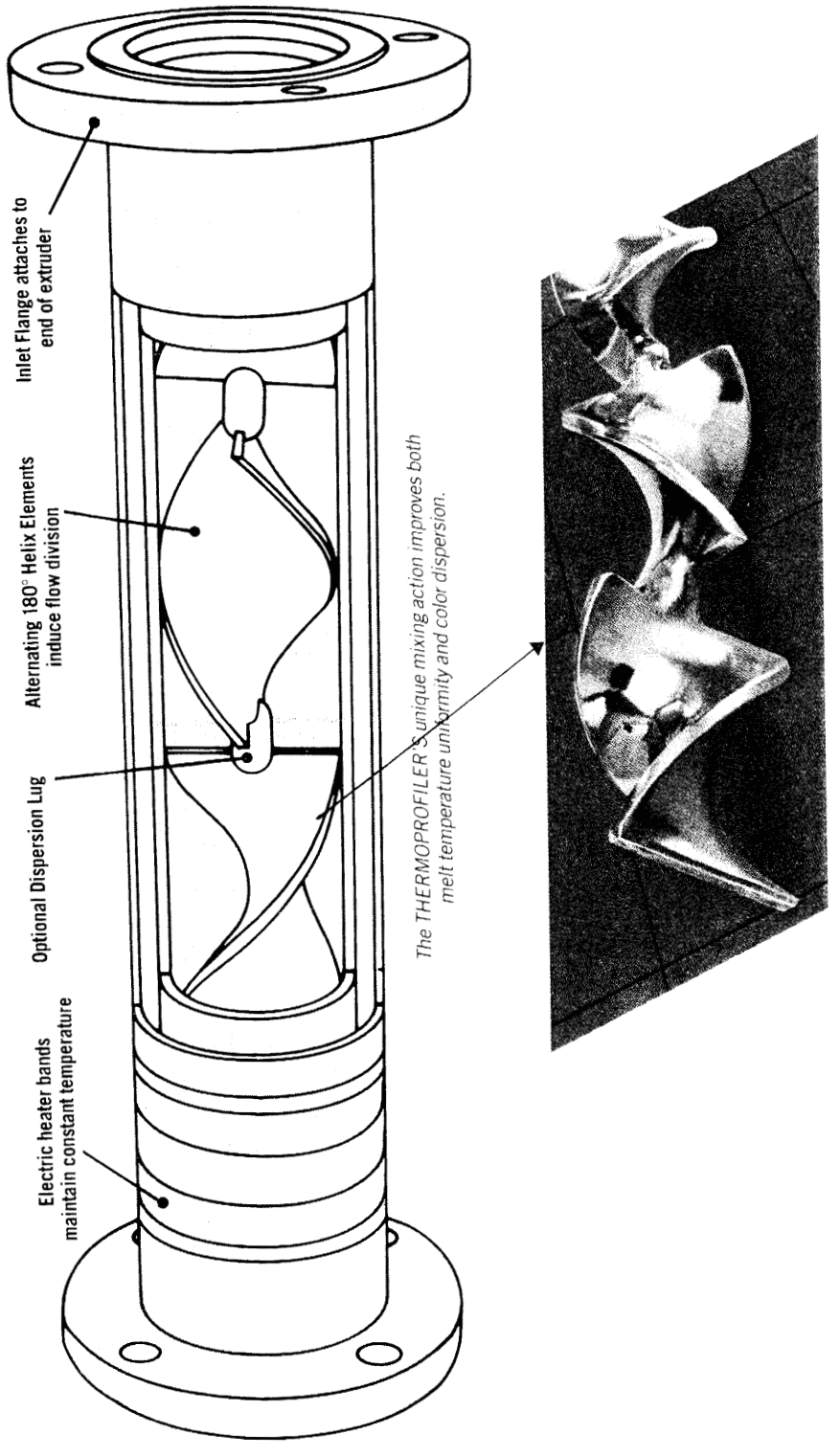

Figure 29 Motionless mixer. (Courtesy of Luwa Corporation.)

the wide screw channel into a number of narrow inlet channels, as shown in Figure 27. Overall, the fluted mixing sections force the material to pass through narrow, albeit short gaps at relatively high shear rates. This should reorient the interfacial area, redistribute the streamlines, increase the total strain imposed, and subject the mixture to high-shear-stress values at the gaps, also introducing some dispersive mixing action.

Another example of a barrier-type device is the Maillefer transition section shown in Figure 28. This is a spiral barrier or secondary screw flight extending over the entire length of the transition section. Many variations of the basic system shown in Figure 28 are possible. Additional barriers or flights can be introduced to split the flow into two or more streams, which in the limit arrives at a series of longitudinal grooves or flutes spaced around the circumference of a cylinder. Mass and force balances on the Maillefer screw is given by Pearson [56].

Dynamic mixing sections like the cavity transfer mixer, can also be incorporated to the single-screw extruder. The cavity transfer mixer facilitates the transfer of the material continuously between the barrel, the "stator," and the screw, the "rotor." This is achieved by the presence of flighted grooves in the barrel, which act as a secondary screw. Over a mixing section the root diameter of the rotor gradually decreases from full depth to zero depth, while the opposite occurs in the stator, forcing the mixture from rotor to stator, and vice versa. This concentric screw effect increases the residence time and the total strain, and further continuously reorients the interfacial area, increasing the efficiency of the extensive mixing.

It is also possible to incorporate distributive mixing sections which do not contain moving parts (i.e., "motionless mixers" to the single screw). The motionless mixers are generally placed between the screw and the die and consist of a string of alternating right- and left-handed helical elements fixed in a tubular housing as shown in Figure 29. The energy for mixing is derived from the pressure loss incurred as the process fluids flow through the motionless mixer. The splitting and recombination of streams results in a predicted increase in the number of striations. The increase in the number of striations with increasing number of elements is shown in Figure 30, with a Luwa motionless mixer. Various types of mixers and their mixing characteristics were recently reviewed [57], where the performances of various motionless mixers were also compared. For example, the number of striations, N_δ, produced with the number of elements present σ vary as the following for various designs:

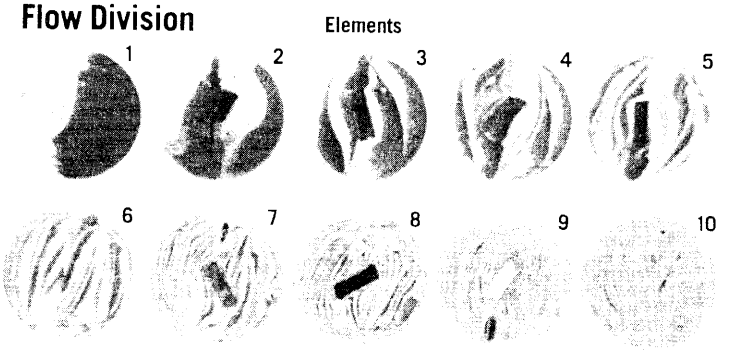

Figure 30 Decrease of striation thickness upon passage through increasing number of elements of a motionless mixer. (Courtesy of Luwa Corporation.)

Kenics mixer: $N_\delta = 2^\sigma$ (35)

ISG: $N_\delta = 4^\sigma$ (36)

Lightnin: $N_\delta = 3(2)^{\sigma-1}$ (37)

Despite their inherent limitations, single-screw extruders are popular mixers mainly because of favorable economics. They are ideal for low-volume compounding jobs, including filling, reinforcing, and coloring of mainly commodity plastics [58]. For tougher applications, including compounding of engineering plastics, and blending of incompatible polymers, twin-screw extruders or single-shaft kneaders with interactive screw and barrel elements are usually employed.

Single-Shaft Kneaders

For dedicated mixing operations such as compounding of poly(vinyl chloride) formulations, molding powders, and reinforced or filled systems, various designs which operate on the basis of a single shaft but are radically different than the conventional plasticating or melt extruder are employed. The common denominators in these single-shaft dedicated compounding extruders are the various protrusions, the grooves, or the profiles built into the barrel sections with corresponding elements in the screw sections. Examples include the Buss and Baker-Perkins Ko-Kneaders, and Sterlex Transfermixer. These mixers are equipped for dispersive mixing, induced through narrow gaps (i.e., high-shear-stress zones and repeated passages through these high-shear-stress zones).

The Ko-Kneader type of continuous kneader is characterized by a kneading screw which rotates and oscillates in a barrel, as shown in Figure 31 [46, 59, 60]. Fluffy feeds (molding powder, etc.) are introduced into the kneader by means of a feeding/cramming screw, which compacts, conveys, and pressurizes the feed into the kneader. The geometry of the kneading screw involves a regular flighted, cooled conveying section adjacent to the hopper exit. The conveying section is followed by the "kneading section." Kneading section involves interrupted flight kneading elements on the screw and barrel surfaces. These are screw flight elements formed by the interruption of the screw spiral by usually three gaps per turn and the kneading teeth, which are fixed on barrel surface. Dispersion

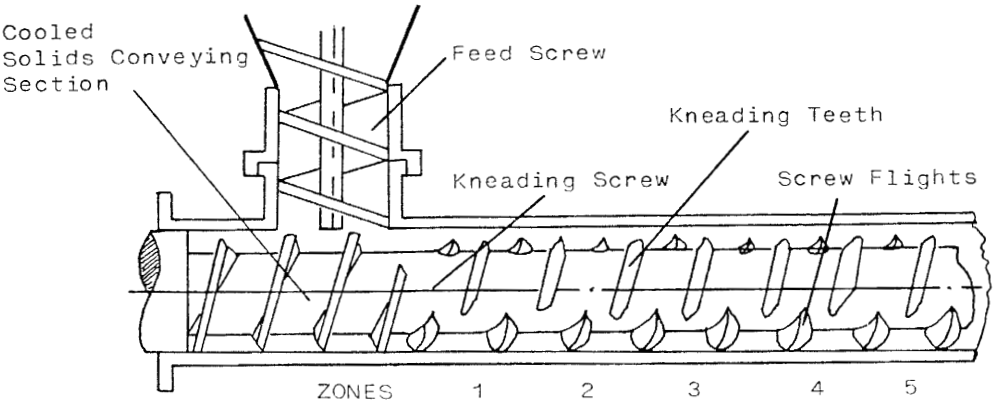

Figure 31 Schematic of a Ko-Kneader.

and homogenization take place in between the rotating and oscillating screw flights and kneading teeth.

The kneading action is illustrated in Figure 32, whereby the interactions of the interrupted screw flights and the barrel kneading teeth are described during one complete screw revolution. Four kneading teeth wipe off all four flanks of a flight during one full turn, and the material is thus subjected to high deformation rates (i.e., dispersive mixing in the small gap between the flight flank and the barrel teeth). Ko-Kneaders are applied in a multitude of processes, including compounding of thermosetting powder coatings (i.e., epoxy, polyester, acrylic, and polyurethane based); thermosetting molding compounds; reinforced engineering plastics with matrices, including PA, PBT, PC, PPS, PPO, and POM; and rigid and plasticized PVC for producing film and sheet.

A mixer that is designed on the cavity mixing principle is the Sterlex Transfermix [61], a double concentric screw extruder. It consists of a rotor within a sectionalized grooved barrel. As shown in Figure 33, the rotor is deep in the feeding section. The prewarming section consists of a smooth barrel section and the melt-mix section incorporates the

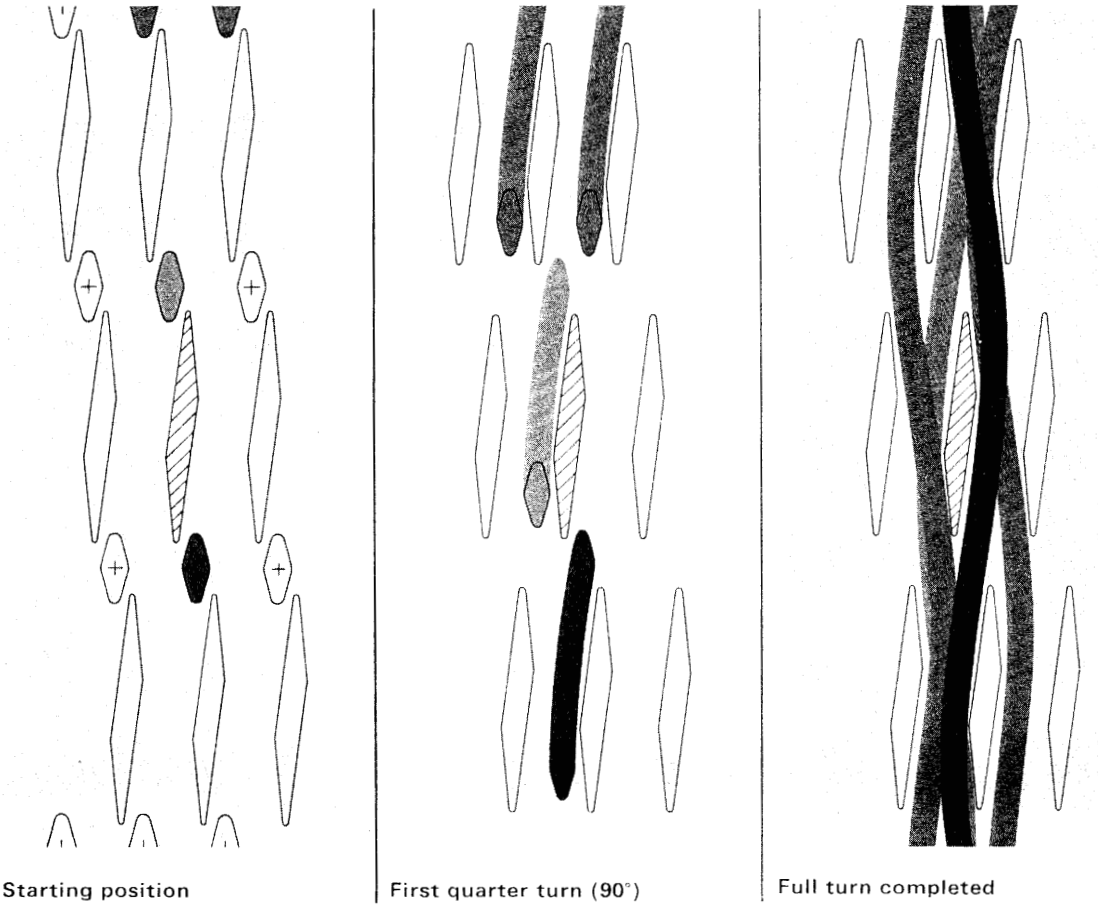

Figure 32 Kneading action in a Ko-Kneader. (Courtesy of Buss Corporation.)

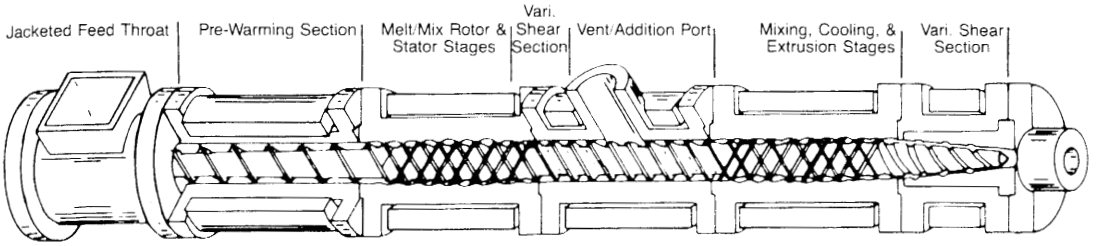

Figure 33 Double concentric screw extruder. (Courtesy of Sterling Corporation.)

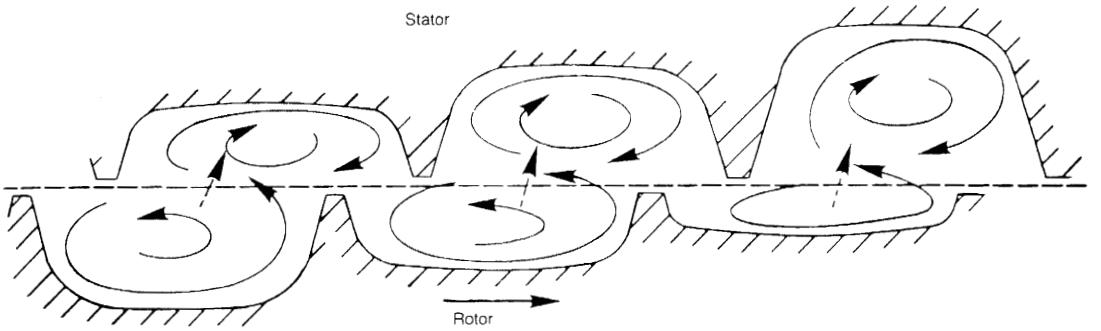

Figure 34 Transfer and mix principle between the stator and the rotor. (Courtesy of Sterling Corporation.)

''transfer and mix'' principle illustrated in Figure 34. There is a conical section at the end of the rotor. The position of the conical section relative to a female bushing is adjustable. The material is forced through the small gap between the rotor and the bushing, thus facilitating dispersive mixing. This mixer is applied in compounding operations, including color concentrates and masterbatches; glass, mica, and talc-filled thermoplastics; plasticized formulations; precharged foamable pellets; and hot-melt adhesives.

A turbine rotor- and stator-based continuous mixer produced by Buss is presented here as an example of mixers applicable to the preparation of solutions, suspensions, pastes, and emulsions. This mixing turbine is shown in Figure 35. It basically involves the inlet and atomization of the solid particles, and the whirling of the particles outward, where they are sprayed with liquid components and continuous downward motion due to the streamlined shapes of the stator and rotor elements and gravity.

Twin-Screw Extruders

There are various types of twin-screw extruders available commercially. They differ in their design and operating principles, thus in their abilities for distributive and dispersive mixing and hence in their application areas. The available twin-screw extruders can be classified as co-rotating and counter-rotating, on the basis of the direction of the rotation of the screws. The counter-rotating extruders can again be classified on the basis of the degree of intermesh of the screws ranging from fully intermeshed, where the flight of one

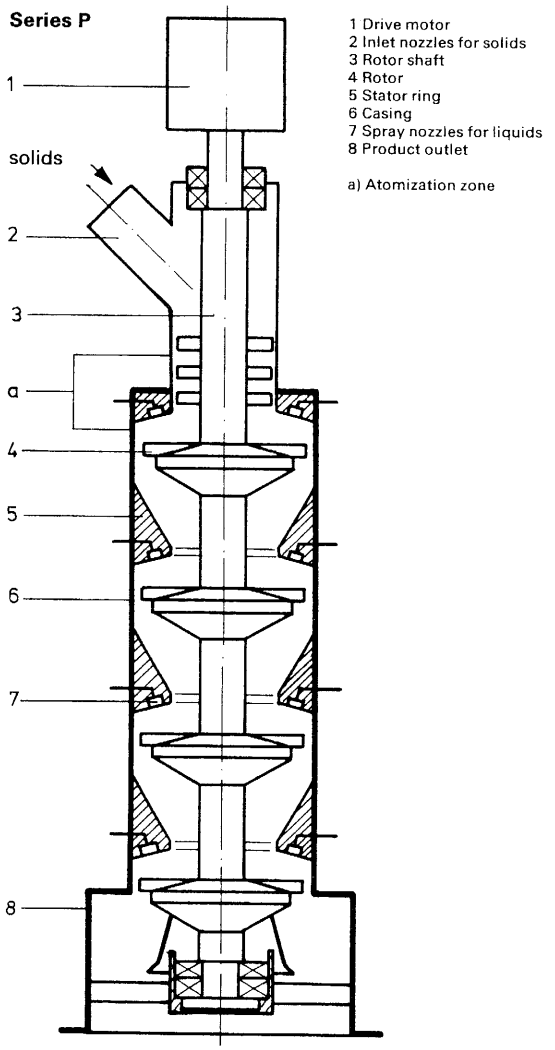

Figure 35 Turbine mixer by Buss. (Courtesy of Buss Corporation.)

screw fits into the channel of the other screw, to nonintermeshing "tangential," where the two screws rotate freely in their barrel sections. The co-rotating screw extruders are not produced in the nonintermeshing mode.

Figure 36 shows the mechanisms of different types of twin-screw extruders. Here distinction is made between the axially open machines, where there is continuous passage between the inlet and outlet and the axially closed machines, where the passage is interrupted at regular intervals. The twin-screw extruders are also classified on the basis of whether or not material exchange between the two screws is possible, neglecting the leakage flows.

The right-handed "forward," regular flighted elements shown in Figure 36 are only one type of element employed in twin-screw extruders. As discussed in individual sec-

Engagement		System	Counter-rotating screw	Co-rotating screw	
intermeshing	fully intermeshing	lengthwise and crosswise closed	1. 	2. theoretically not possible	
		lengthwise open and crosswise closed	3. theoretically not possible	screws	4. 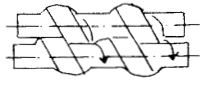
		lengthwise and cross-wise open	5. theoretically possible practically not realized	kneading discs	6. 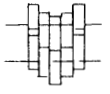
	partially intermeshing	lengthwise open and crosswise closed	7. 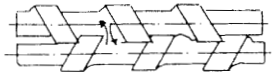	8. theoretically not possible	
		lengthwise and crosswise open	9a 	10a 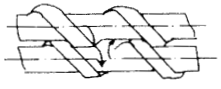	
			9b 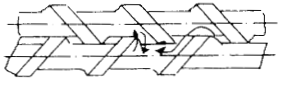	10b 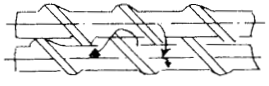	
not intermeshing	not intermeshing	lengthwise and crosswise open	11. 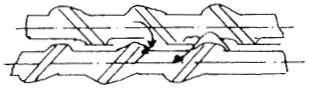	12. 	

Figure 36 Types of twin-screw extruders. (From Ref. 62.)

tions, twin-screw extruders can also be equipped with other types of elements, including left-handed, "reverse" regular flighted elements, forward and reverse kneading discs, shearing discs, and so on. Thus most twin-screw extruder screws can be assembled with the "building-block" principle. Depending on the requirements of the compounding task at hand, proper screw elements can be selected and assembled.

Counter-Rotating Intermeshing Twin-Screw Extruders

The available counter-rotating intermeshing twin-screw extruders are designed as "conical" and "cylindrical" extruders [63]. Conical twin-screw extruders allow for more space for the installation of thrust bearings. On the other hand, cylindrical counter-rotating twin-screw extruders enjoy the ability to be built by the building-block method.

Schematic representation of the cylindrical intermeshing counter-rotating screws is shown in Figure 37. Bulk of the material is conveyed in the down-channel direction in isolated C-shaped segments, with the flights acting as positive-displacement pumps [62–67]. The unwound channel is shown in Figure 38, whereby the material circulates both in the down-channel, z, and cross-channel, x, directions. Neglecting leakage flow, the volumetric flow rate, Q, is given as a function of screw speed, N, and the geometry alone [1]:

$$Q = \pi N \bar{D} L_s H \left[1 - \frac{1}{2\pi} \frac{D_f}{\bar{D}} \frac{D_f}{H} \cos^{-1}\left(1 - \frac{H}{D_f}\right) + \frac{1}{2\pi} \frac{D_f}{\bar{D}} \left(1 - \frac{H}{D_f}\right) \sqrt{\frac{2D_f}{H} - 1} \right] \tag{38}$$

where

L_s = screw lead
H = channel depth

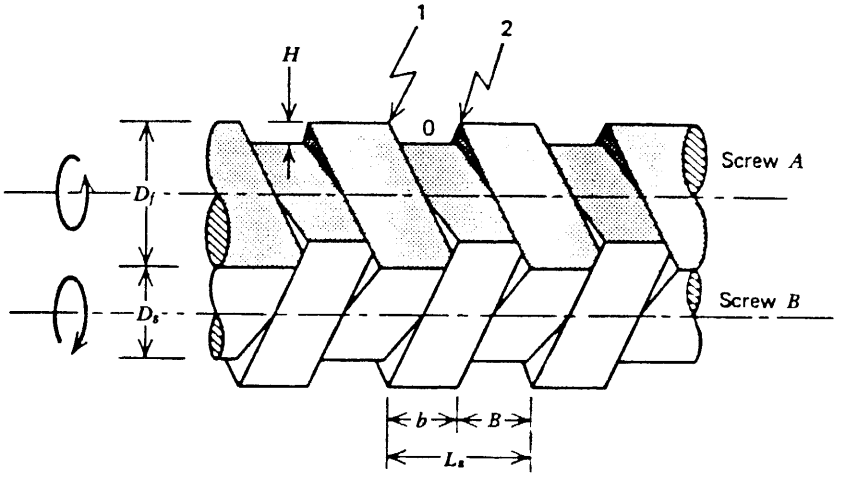

Figure 37 Schematic representation of intermeshing counter-rotating twin-screw extruder. (From Ref. 1.)

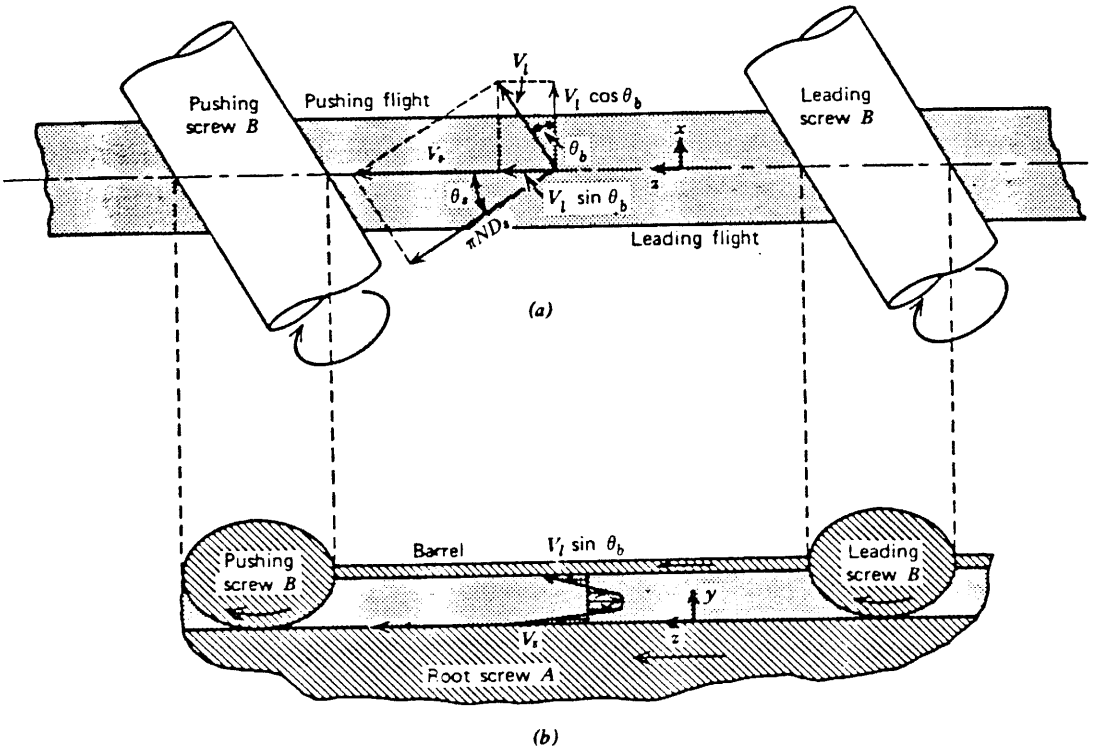

Figure 38 Unwound channel of counter-rotating screw. (From Ref. 1.)

D_f = diameter at the tip of flights

$\bar{D}$ = mean diameter, $D_f - H$

Thus, in the absence of leakage flow, the residence-time distribution in the intermeshing counter-rotating mode should be very narrow, with the average residence time, θ, becoming

$$\theta = \frac{Q}{V} \tag{39}$$

where V is the volume of the extruder. The volumetric flow rate, Q, is commonly controlled through starve feeding in twin-screw extruders. Flood feeding generally requires prohibitively high torque and power.

The typical circulatory flow pattern is shown in Figure 39 and suggests continuous extensive mixing of the material as it is being pushed by the screw flight and is being dragged by the barrel and the screw root. It should be noted further that leakage flows exist in intermeshing counter-rotating twin-screw extruders [65, 67] and are shown schematically in Figure 40. The leakage flows occur through the screw flight and the barrel, Q_f, between the flanks of the flights, Q_t and Q_s, and between the tip of the flight of one screw and the root of the second screw, Q_c. The leakage flows induce the following:

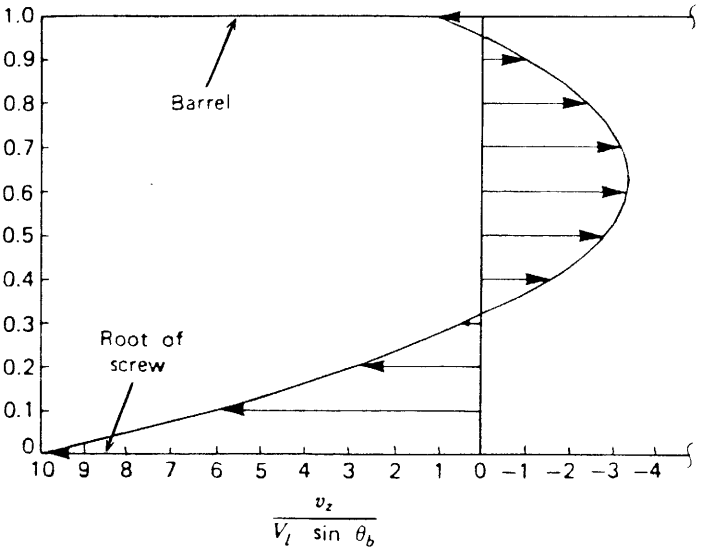

Figure 39 Velocity profile in the down-channel and cross-channel direction in regular forward flighted counter-rotating twin screw. (From Ref. 1.)

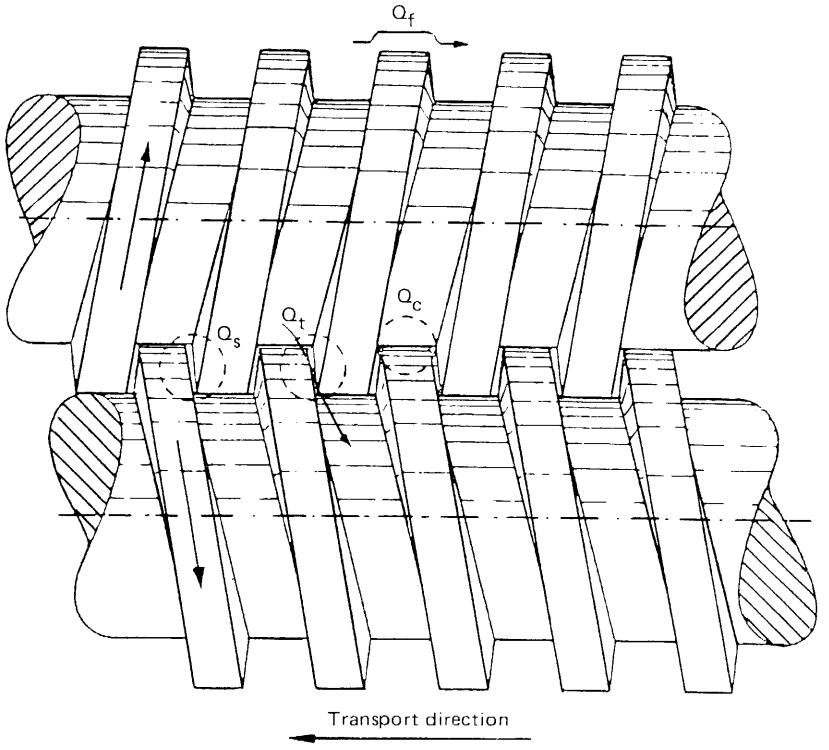

Figure 40 Leakage flows in intermeshing counter-rotating twin screw.

1. Intermingling of the material elements located in different C-shaped segments at the same screw and in between different screws. This should generate backmixing and broaden the residence time.
2. The passage of the material through the narrow gaps during leakage, where the deformation rates are relatively high, generates dispersive mixing.
3. The leakage flow, in between the tip of one screw flight and the root of the second screw, whereby the material is calendered, generates normal stresses that tend to push the two screws apart. The parting forces can generate considerable wear and thus limit the intermeshing counter-rotating twin-screw extruders to relatively low screw speeds, typically less than 200 rpm [68].

The current applications of counter-rotating twin-screw extruders include tasks that require narrow residence times (i.e., PVC profile extrusion and other applications), including color-concentrate preparation, and possibly as drag-induced flow reactors [69] (i.e., reactive processing).

Counter-Rotating Nonintermeshing (Tangential) Twin-Screw Extruders

The schematics of the regular flighted, forward screw elements in tangential extruders is shown in Figure 41. The two screws rotate at the same frequency and the respective flights can be placed either facing each other or in a staggered fashion. The kinematics of the flow is not very different than the one in the single-screw extruder, except for one important difference, the interaction between the two screws. The unwound channel is shown in Figure 42, with a corresponding three-plate model. The lower and upper plates represent the two screws, and the moving slitted center plate represents the barrel surface for both screws. At the slit, the presence of a pressure gradient will act as a driving force for interchange of material between the two screws with pressure flow. The design equation for the tangential extruder for isothermal flow of Newtonian fluids in shallow channels becomes

$$Q = \frac{1}{2} WHV_{bz}F_1 - \frac{WH^3}{12\eta}\frac{\Delta P_T}{\Delta Z_T}F_2 \tag{40}$$

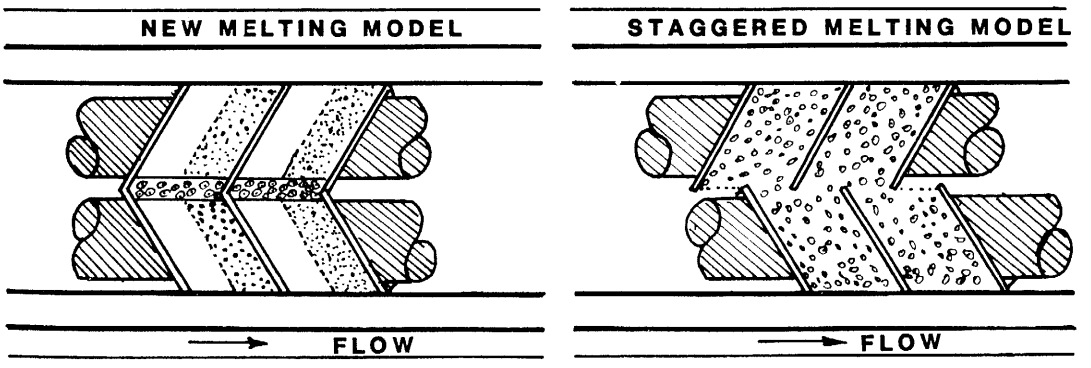

Figure 41 Matched and staggered screw-flight positions in tangential twin screw. (From Ref. 70.)

where

W = channel width
H = depth
ΔP_T = pressure change over total helical distance, ΔZ_T
η = Newtonian viscosity
F_1, F_2 = correction factors to account for the slit opening

The expected velocity profile is shown again in Figure 42.

The meeting of the streams at the interface between the two screws increases the efficiency of extensive mixing in the counter-rotating twin-screw extruders, in comparison to single-screw extruders. It has been shown experimentally that the leakage flow at the nip can penetrate and form reoriented regions across the depth of the channel [71]. If the flights are further staggered, as shown in Figure 41, this mode should give rise to

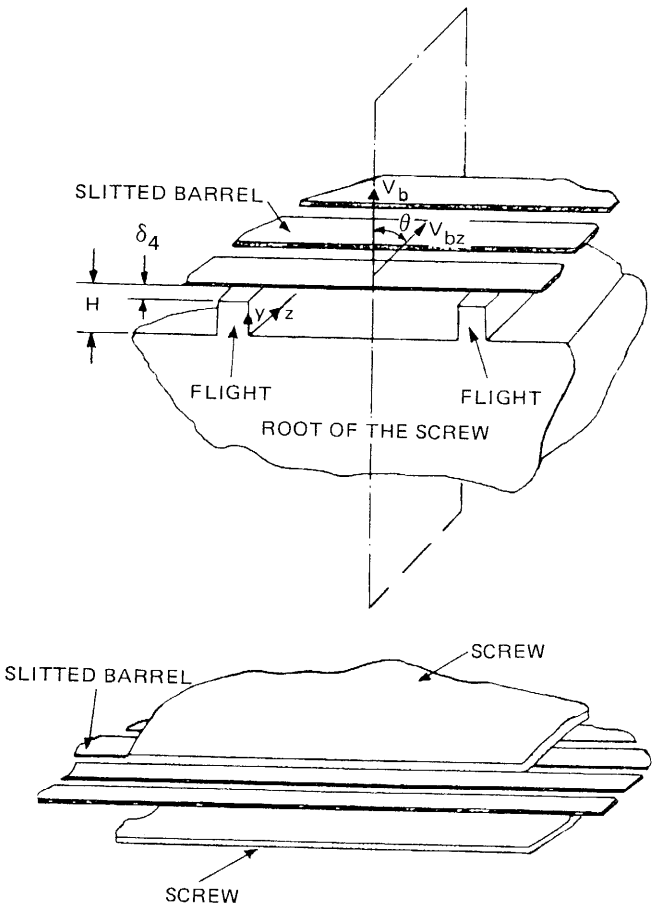

Figure 42 Unwound channel in nonintermeshing counter-rotating twin-screw extruder. (From Ref. 70.)

better extensive mixing at the expense of decrease in pumping efficiency. The residence-time distribution of a nonintermeshing twin-screw extruder is determined experimentally to be broader than the single screw [72], presumably due to excessive leakage flows outlined above.

Other types of elements applicable to tangential extruders are shown in Figure 43, and include reverse flighted and cylindrical elements. The reverse flighted elements should induce extensive mixing in the longitudinal direction and cylindrical elements are used for sealing purposes close to liquid addition ports.

Counter-rotating nonintermeshing tangential twin-screw extruders are employed for applications that do not necessitate dispersive mixing. The applications include polymerization reactions, blending of some polymers, compounding for hot-melt adhesives, pigment concentrates, incorporation of glass-fiber reinforcements into engineering plastics, and devolatilization.

Co-rotating Intermeshing Twin-Screw Extruders

Co-rotating twin-screw extruders are commonly produced only on the fully intermeshing mode and operate on the building-block principle. Screw elements are selected and assembled depending on the requirements of the mixing task at hand. Some of the employed screw elements are shown in Figure 44. Commonly employed elements include right-handed and left-handed (forward and reverse) regular flighted elements, forward and reverse kneading discs, and mixing and shearing pins. Obviously, various elements come in with various shapes and dimensions also. Reviews of the operation principals and comparisons especially to counter-rotating twin-screw extruders are available [62, 74–79].

For regular flighted elements, fully intermeshing co-rotating screws are open lengthwise but are closed crosswise, except for leakage over the flights. The analysis of right-handed regular flighted elements of the intermeshing co-rotating twin-screw extrusion process is not different from the single-screw except for the nip regions, where the two screws intermesh. The schematic of the process is shown in Figure 45, where the two flights are assumed to move vertically up and down at the nip region.

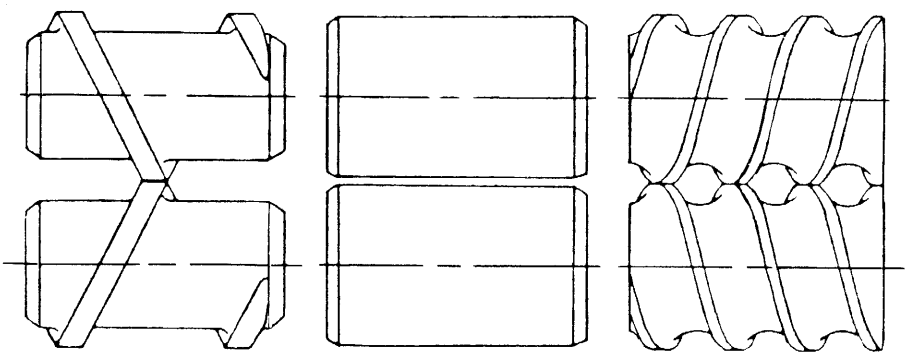

Figure 43 Various types of elements used in nonintermeshing counter-rotating twin-screw extruders. (From Ref. 73.)

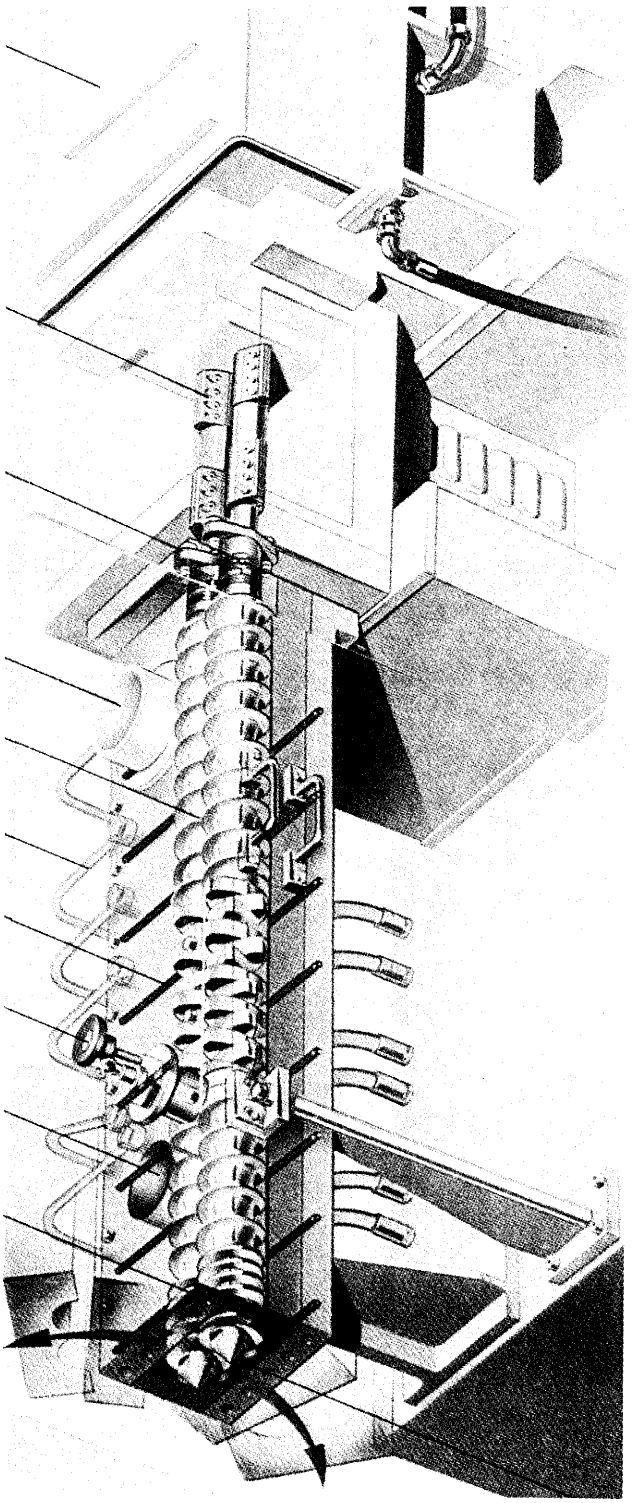

Figure 44 Co-rotating twin-screw extruder. (Courtesy of Baker-Perkins.)

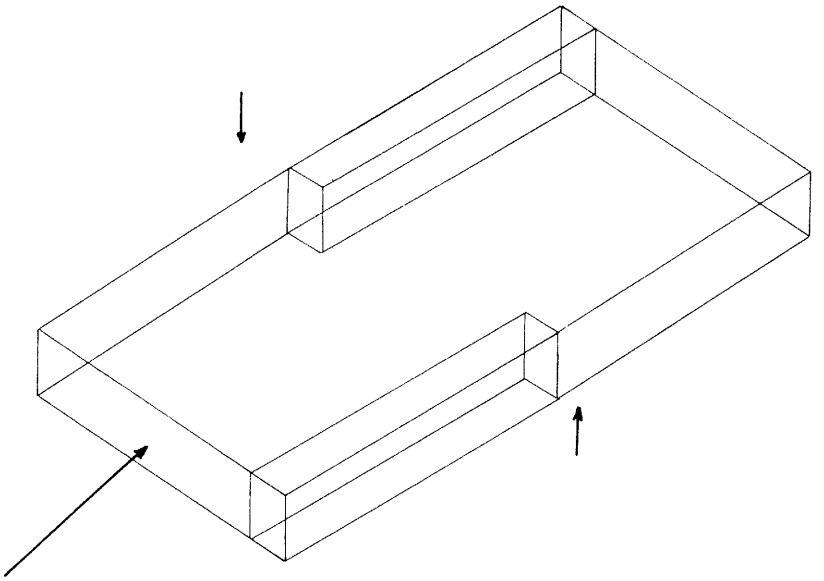

Figure 45 Schematic of flow in regular flighted co-rotating twin-screw section. (From Ref. 80.)

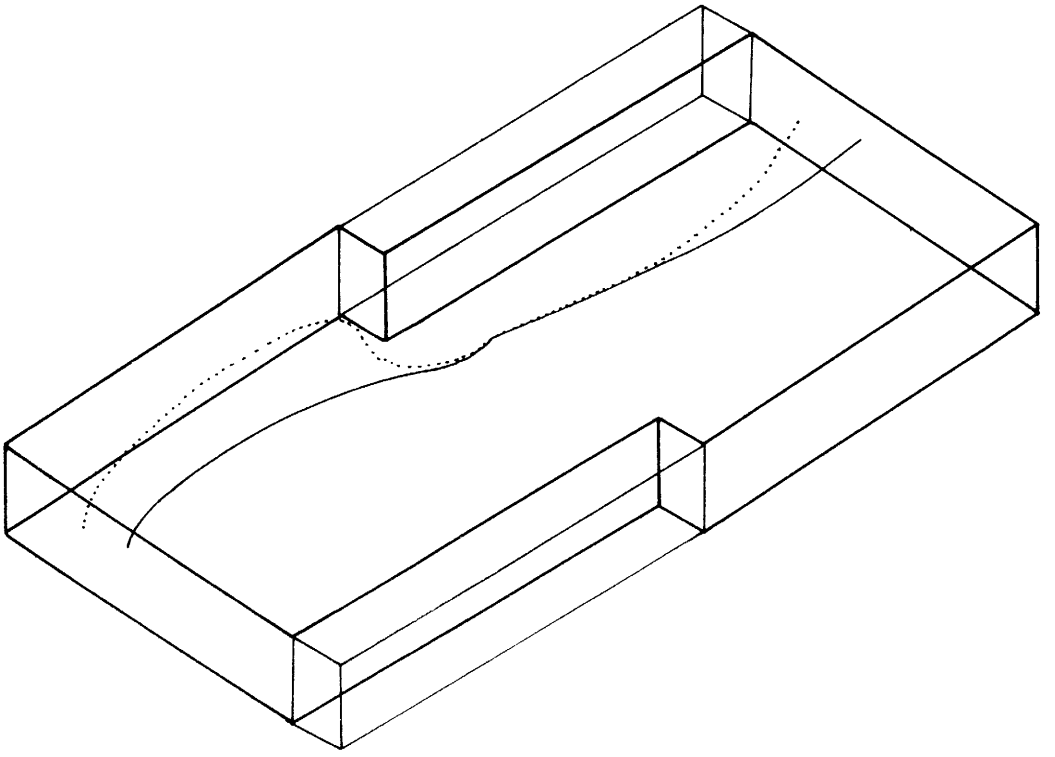

Figure 46 Change in direction in the nip region in co-rotating flow. (From Ref. 80.)

Our three-dimensional finite-difference-based solution of the continuity and momentum conservation equations suggest that the nip area serves to:

1. Change the direction of the shearing planes, thus to reorient the interfacial area for better extensive mixing.
2. Impart relatively high rates of shear. The relative velocity at the interface is relatively high, given by $2\pi N(R_s + R_f)$, where N is rotational speed of the screws, and R_s and R_f are the radii at the screw root and at the tip of the flights, respectively.

The change in direction at the nip area and the distribution of deformation rate (i.e., the second invariant of deformation rate tensor at a location away from the nip area and at the nip area) are shown in Figures 46 and 47. The length of arrows are proportional to the value of the second invariant. The deformation field can be affected significantly if the widths of the flights are changed.

Some of the "lenticular-shaped" kneading discs [81] that can be incorporated into the

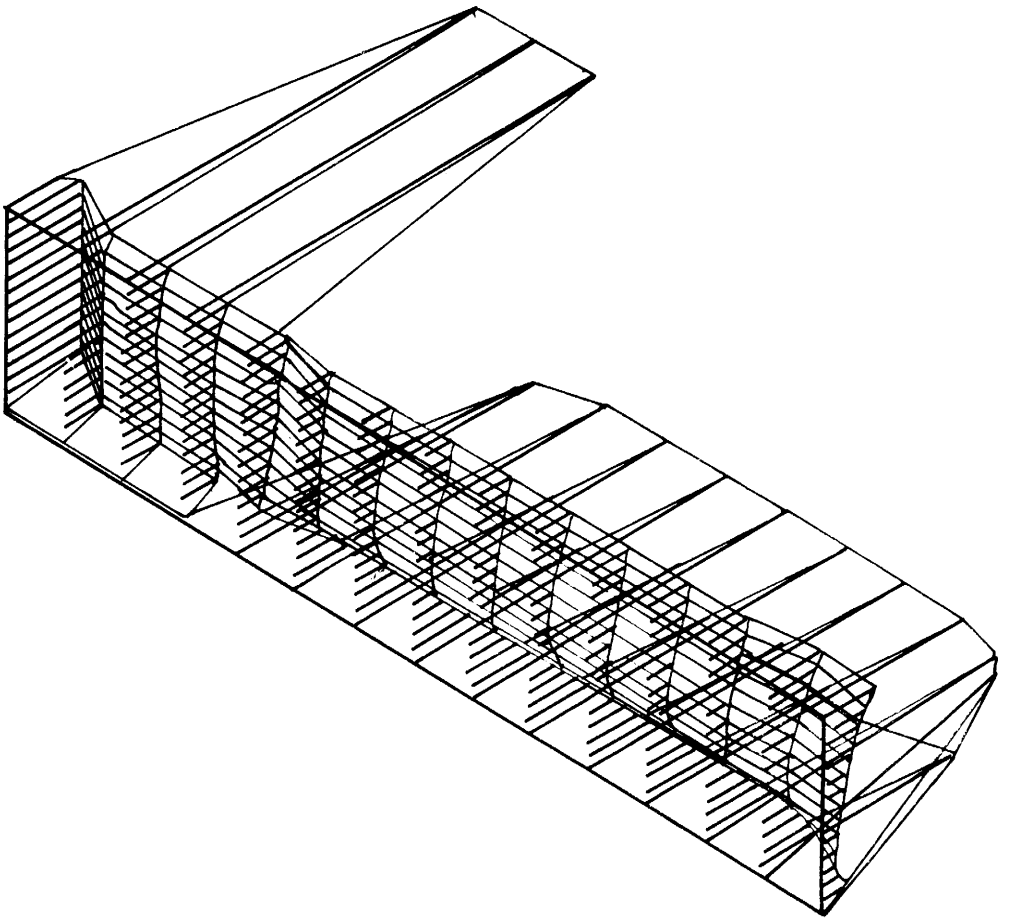

Figure 47 Rate of deformation in the nip region in co-rotating flow. (From Ref. 80.)

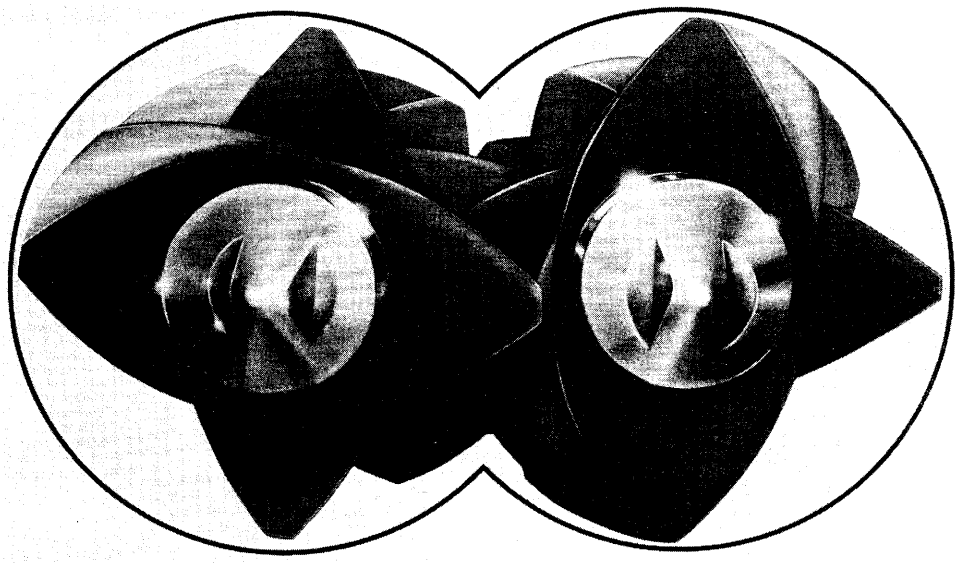

Figure 48 Kneading disks in co-rotating twin-screw extruders. (Courtesy of Werner & Pfleiderer.)

screw are shown in Figure 48. The discs are self-wiping as long as they are staggered at 90° angles as shown. Depending on the stagger angle neutral, forward or reversing screw sections can be generated. In the neutral mode, the material is transferred from one half of the barrel to the other half in figure-eight form before being pressured to move on in the axial direction by the following melt elements. The calendering action (i.e., passage of the material through the high-shear-rate gap between the two discs) generates excellent dispersive mixing. The introduction of reverse elements will generate further extensive mixing in the axial direction.

Co-rotating twin-screw extruders are widely used currently for a multitude of applications, including incorporation of fillers and reinforcements to commodity plastics and engineering resins, mixing in production of powder coatings, additive concentrates, color concentrates, thermosetting molding compounds, thermoplastic rubbers, blowing agent compounding, polymer blending, PVC formulations, and reactive extrusion. They are also employed widely in other industries, including the cooking, mixing, and processing of food products.

Other Continuous Mixers

The common feature of all the continuous mixers reviewed is the presence of one moving boundary and one stationary surface in the channel (the screw and the barrel). One continuous mixer, the Farrell Diskpack, is a co-rotating disc extruder and has two moving drag-inducing surfaces [82–85]. The machine schematically shown in Figure 49 consists of a single rotor with toroidal (doughnut-shaped) processing chambers, which fit in a circular housing. Between the inlet and outlet openings of each chamber, a channel block is positioned as a stationary element. It diverts the polymer through the outlet. Processing

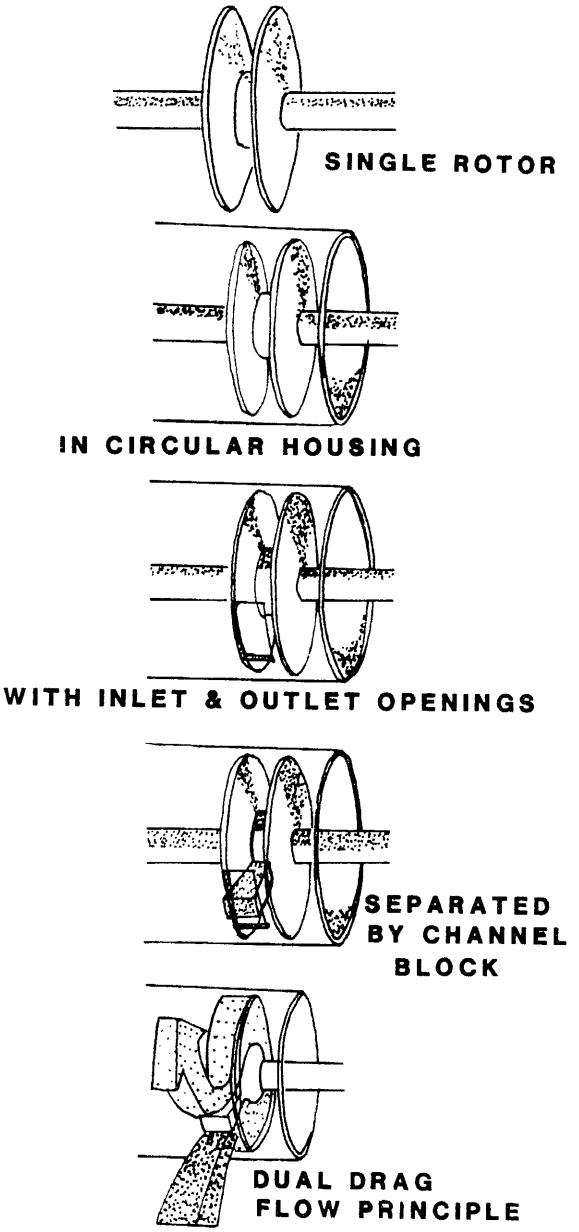

Figure 49 Co-rotating disc extruder. (Courtesy of Farrel Corporation.)

chambers may be connected in parallel, in series, or in combination and are assembled on the building-block principle. Elements can be introduced through the housing to enhance mixing, polymer film spreading, and liquid injection.

The flow kinematics in the chamber can be analyzed on the basis of Newtonian, isothermal, fully developed flow. The analysis is similar to that developed for unwound single-screw extruder channels, except that now both walls are moving with velocity V_0. Including the pressure flow, which arises due to the presence of a flow restriction (i.e., die downstream), the design equation becomes [1]

$$q = V_0 H - \frac{H^3}{12\eta}\frac{dp}{dz} \tag{41}$$

where

q = volumetric flow rate per width

H = depth of the channel, which has both walls moving at velocity V_0

dp/dz = pressure gradient due to the presence of a restriction

The ratio of the drag and pressure-induced flow rates is given by

$$\frac{q_p}{q_d} = \frac{H^2}{12\eta V_0}\frac{dp}{dz} \tag{42}$$

The velocity distribution for this simplified analysis is shown in Figure 50 for various values of q_p/q_d. As expected, the presence of the restriction generates a circulatory flow in the axial direction. At the same pressurization capability, the shear rates with two walls moving are considerably smaller than with only one wall moving. Thus mixing pins are

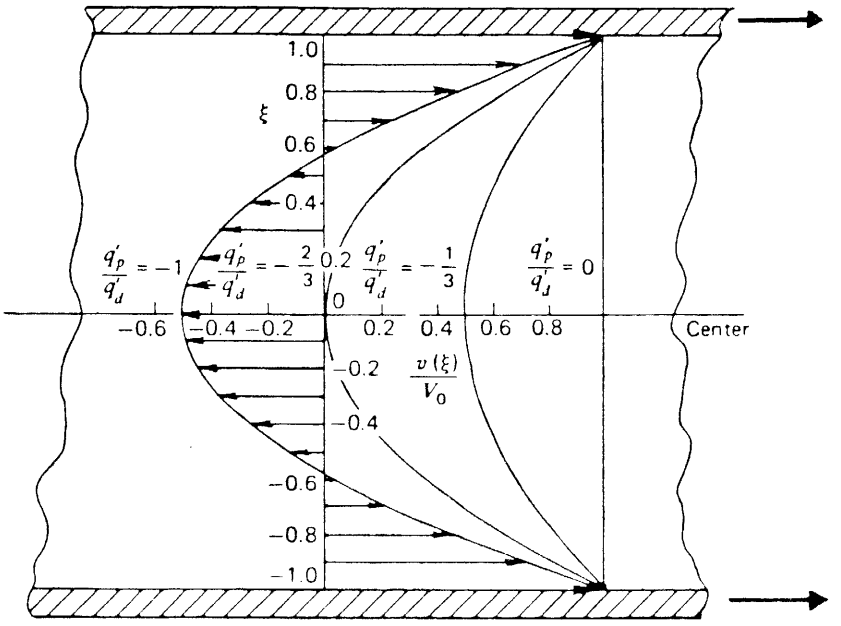

Figure 50 Velocity profiles in co-rotating disc extruder. (From Ref. 1.)

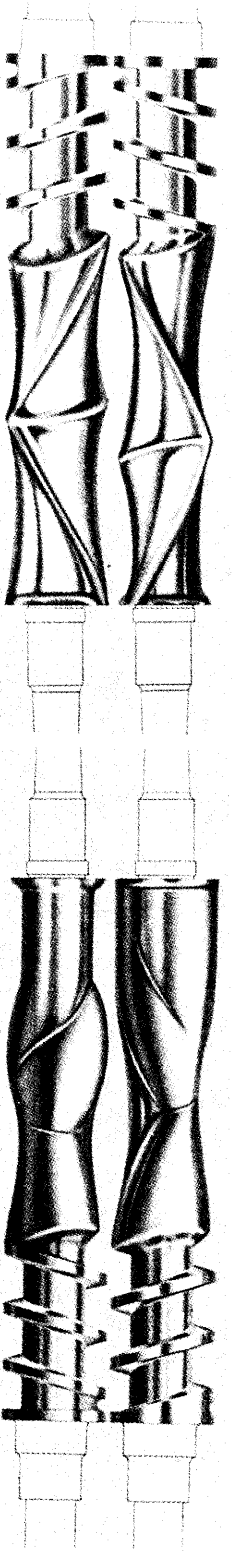

Figure 51 Twin-rotor internal mixer. (Courtesy of Farrel Corporation.)

necessary to impose high strains and to reorient the melt. High-shear-stress regions may also be introduced for dispersive mixing. This type of compounder is applied in the compounding of commodity and engineering plastics with fillers and reinforcing agents, in preparation of concentrates, and in polymer blending and alloying.

Finally, the Farrel continuous mixer is a twin-rotor internal mixer [86] and is based on the transformation of the popular Banbury batch mixer into a continuous mode. Perpendicular to the axis of rotation of the rotors, the cross section of this continuous mixer resembles the batch Banbury mixer [1]. This mixer, shown in Figure 51, basically involves a conveying section, which propels the ingredients and an intensive mixing section. In the intensive mixing section the material is dispersed by passage through small gaps found between the rotors and the chamber walls, coupled with kneading between the rotors and a rolling action of the material itself. This continuous mixer is applied in polyolefin homogenization and masterbatching, crosslinking of polyethylene, compounding of PVC, polyamid, ABS, SAN, carbon electrode stock, TRP, rubbers, and in the preparation of concentrates and additives.

REFERENCES

1. Z. Tadmor and C. G. Gogos, *Principles of Polymer Processing*, Wiley, New York (1979).
2. I. Manas-Zloczower, A. Nir, and Z. Tadmor, *Rubber Chem. Techn., 57*: 583–620 (1984).
3. W. D. Mohr, in *Processing of Thermoplastic Materials* (E. Bernhardt, ed.), R. E. Krieger, Melbourne, Fla. (1959).
4. J. M. McKelvey, *Polymer Processing*, Wiley, New York (1962).
5. P. Danckwerts, *Appl. Sci. Res., Sect. A, 3*: 279–296 (1952).
6. R. S. Spencer and R. M. Wiley, *J. Colloid Sci., 6*: 133–145 (1951).
7. K. Ng and L. Erwin, *Polym. Eng. Sci., 21*: 212–217 (1981).
8. L. Erwin, *Polym. Eng. Sci., 18*: 572 (1978).
9. B. Bird, R. Armstrong, and O. Hassager, *Dynamics of Polymeric Liquids*, Vol. 1, Wiley, New York (1977).
10. G. Taylor, *Proc. R. Soc. Ser. A, 138*: 41–48 (1932).
11. G. Taylor, *Proc. R. Soc. Ser. A, 146*: 501–523 (1934).
12. F. Rumscheidt and S. Mason, *J. Colloid Sci., 16*: 238–261 (1961).
13. W. Bartok and S. Mason, *J. Colloid Sci., 6*: 354 (1961).
14. G. Chaffey and S. Mason, *J. Colloid Interface Sci., 21*: 254 (1966).
15. H. Karam and J. Bellinger, *Ind. Eng. Chem. Fundam., 7*: 576 (1968).
16. R. Cox, *J. Fluid Mech., 37*: 601 (1969).
17. S. Torza, R. Cox, and S. Mason, *Phil. Trans. Roy. Soc., 269*: 295 (1971).
18. S. Torza, R. Cox and S. Mason, *J. Colloid Interface Sci., 38*: 395–411 (1972).
19. R. Flumerfelt, *Ind. Eng. Chem. Fundam., 11*(3): 312–318 (1972).
20. H. Van Oene, *J. Colloid Interface Sci., 40*: 448–467 (1972).
21. A. Acrivos and T. Lo, *J. Fluid Mech., 86*(4): 641–672 (1978).
22. D. Chan and R. Powell, *J. Non-Newton. Fluid Mech., 15*: 165–179 (1984).
23. K. Kitano, T. Kataoka, and Y. Nagatsuka, *Rheol. Acta, 23*: 408–416 (1984).
24. I. Manas-Zloczower, A. Nir, and Z. Tadmor, *Rubber Chem. Technol., 55*: 1250 (1982).
25. P. Hold, *Adv. Polym. Technol., 2*: 141–151 (1982).
26. W. Bolen and R. Colwell, *Soc. Plast. Eng. J., 14*: 24–28 (1958).
27. E. Dizon, E. Micek, and C. Scott, *Rubber Chem. Technol., 48*: 339 (1975).
28. R. Bird, H. Warner, Jr., and D. Evans, *Fortsch. Hochpolym. Forch., 8*: 1–90 (1971).
29. Z. Tadmor, *Ind. Eng. Chem. Fundam., 15*: 346 (1976).
30. D. Kalyon and D. Yu, unpublished results (1986).
31. J. White, R. Ufford, K. Dharod, and R. Prise, *J. Appl. Polym. Sci., 16*: 1313–1330 (1972).

32. G. Akay, *Rheol. Acta, 18*: 256–267 (1979).
33. R. Jones, *Rheol. Acta, 14*: 397–401 (1975).
34. F. Gauthier, H. Goldsmith, and S. Mason, *Trans. Soc. Rheol., 15*: 297–330 (1971).
35. G. Segre and A. Silberberg, *Nature, 189*: 209 (1961).
36. G. Segre and A. Silberberg, *J. Fluid Mech., 14*: 115 (1962).
37. C. Denson, E. Christiansen, and D. Salt, *AIChE J., 12*: 589–595 (1966).
38. U. Yilmazer, C. Gopos, and D. Kalyon, paper submitted to *Polym. Comp.*, June (1988).
39. A. Metzner, *J. Rheol., 29*: 739–775 (1985).
40. D. Kalyon and M. Khemis, *SPE ANTEC Tech. Pap., 30*: 136–140 (1984).
41. D. Kalyon and M. Khemis, *Plast. Rubber Process. Appl. 8*: 157–164 (1987).
42. R. Nichols and G. Kinder, *SPE ANTEC Tech. Pap., 20* (1974).
43. J. McKelvey, *Plast. Eng.*, 45–49 (June 1978).
44. L. Lopez-Latorre and J. McKelvey, *Adv. Polym. Technol., 3*(4): 355–364 (1983).
45. Z. Tadmor and E. Broyer, *Polym. Eng. Sci., 12*(5): 379 (1972).
46. D. Kalyon and M. Hallouche, *Adv. Polym. Technol., 6*: 237–249 (1986).
47. A. Gotsis, D. Kalyon, C. Gogos, and C. Tsenoglou, unpublished results (1987).
48. W. Mohr, R. Saxton, and C. Jepson, Ind. Eng. Chem., 49: 1855 (1957).
49. G. Pinto and Z. Tadmor, *Polym. Eng. Sci., 10*(5): 279–288 (1970).
50. D. Wolf and D. White, *AIChE J., 22*: 122–131 (1976).
51. R. Chella and J. Ottino, *Ind. Eng. Chem. Fundam., 24*: 170–180 (1985).
52. F. Mokhtarian and L. Erwin, *Polym. Eng. Sci., 23*: 49 (1983).
53. B. Maddock, *SPE J.* (23 July 1967).
54. C. Rauwendaal, *SPE ANTEC Tech. Pap., 30*: 62 (1984).
55. R. Espesito, *Plast. Eng.*, 39 (Oct. 1986).
56. J. Pearson, *Mechanics of Polymer Processing*, Elsevier, London, p. 662 (1985).
57. J. Godfrey, in *Mixing in the Process Industries* (N. Harnby, M. Edwards, and A. Nienow, eds.), Butterworth, Sevenoaks, Kent, England (1985).
58. V. Wigotsky, *Plast. Eng.*, Feb. 19–23 (1986).
59. K. Stade, *Polym. Eng. Sci., 17*: 50 (1977).
60. K. Stade, *Polym. Eng. Sci., 18*: 107 (1978).
61. C. Parshall and P. Geyer, U.S. Pat. 2,744,287 (1956).
62. H. Herrmann, U. Burkhardt, and S. Jakopin, *SPE Tech. Pap.*, Montreal (1977).
63. C. Rauwendaal, *Polym. Eng. Sci., 21*(16): 1092–1100 (1981).
64. C. Wyman, *Polym. Eng. Sci., 15*: 606–611 (1975).
65. L. Janssen, K. Mulders, and J. Smith, *Plast. Polym.*, 93–98 (June 1975).
66. G. Schenkel, *Plastics Extrusion Technology and Theory*, Iliffe, London (1966).
67. Z. Doboczky, *Plastverarbeiter, 16*: 57–67 (1965).
68. R. Nichols, *Mod. Plast.*, 90–94 (Sept. 1986).
69. L. Janssen and B. Schaart, *2nd World Congress of Chemical Engineering*, Montreal, vol. 6, p. 543 (1981).
70. A. Kaplan and Z. Tadmor, *Polym. Eng. Sci., 14*: 58–66 (1974).
71. C. Howland and L. Erwin, *SPE ANTEC Tech. Pap., 29*: 113–116 (1983).
72. C. Walk, *SPE ANTEC Tech. Pap., 28*: 423 (1982).
73. R. Nichols and J. Yao, *SPE ANTEC Tech. Pap., 28*: 416 (1982).
74. W. Mack and R. Herter, *Chem. Eng. Prog.*, 64–70 (Jan. 1976).
75. K. Eise, H. Herrmann, H. Werner, and U. Burkhardt, *Adv. Plast. Technol., 1*(2): 1–22 (1981).
76. D. Todd, *Polym. Eng. Sci., 15*(6): 437–443 (1975).
77. D. Todd and D. Baumann, *Polym. Eng. Sci., 18*(4): 321–325 (1978).
78. D. Kalyon, A. Gotsis, C. Gopos, and C. Tsenoglou, *SPE ANTEC Tech. Pap., 34*: 64–66 (1988).
79. M. Booy, *Polym. Eng. Sci., 18*: 973 (1978).

80. C. Du, ChE 800 Special Research Thesis, Stevens Institute of Technology, Hoboken, New Jersey (March 1987).
81. B. Loomans and A. Brennan, U.S. Pat. 3,195,868 (1965).
82. Z. Tadmor, P. Hold, and L. Valsamis, *SPE ANTEC Tech. Pap.*, *25*: 193–204 (1979).
83. Z. Tadmor, P. Hold, and L. Valsamis, *SPE ANTEC Tech. Pap.*, *25*: 205–211 (1979).
84. Z. Tadmor, U.S. Pat. 4,142,805 (1979).
85. Z. Tadmor, U.S. Pat. 4,194,841 (1980).
86. P. Hold, U.S. Pat. 3,154,808 (1969).